2009

Numerical Study Of Encapsulated Phase Change Material (epcm) Slurry Flow In Microchannels

Sarada Kuravi
University of Central Florida

NUMERICAL STUDY OF ENCAPSULATED PHASE CHANGE MATERIAL (EPCM) SLURRY FLOW IN MICROCHANNELS

by

SARADA KURAVI
M.S. University of Central Florida, 2006
B. Tech. Jawaharlal Nehru Technological University, 2002

A dissertation submitted in partial fulfillment of the requirements
for the degree of Doctor of Philosophy in Mechanical Engineering
in the Department of Mechanical, Materials and Aerospace Engineering
in the College of Engineering and Computer Science
at the University of Central Florida
Orlando, Florida

Summer Term
2009

Major Professor: Louis Chow

ABSTRACT

Heat transfer and flow characteristics of phase change material slurry flow in microchannels with constant heat flux at the base were investigated. The phase change process was included in the energy equation using the effective specific heat method. A parametric study was conducted numerically by varying the base fluid type, particle concentration, particle size, channel dimensions, inlet temperature, base heat flux and melting range of PCM. The particle distribution inside the microchannels was simulated using the diffusive flux model and its effect on the overall thermal performance of microchannels was investigated. Experimental investigation was conducted in microchannels of 101 μm width and 533 μm height with water as base fluid and n-Octadecane as PCM to validate the key conclusions of the numerical model.

Since the flow is not fully developed in case of microchannels (specifically manifold microchannels, which are the key focus of the present study), thermal performance is not as obtained in conventional channels where the length of the channel is large (compared to length of microchannels). It was found that the thermal conductivity of the base fluid plays an important role in determining the thermal performance of slurry. The effect of particle distribution can be neglected in the numerical model under some cases. The performance of slurry depends on the heat flux, purity of PCM, inlet temperature of the fluid, and base fluid thermal conductivity. Hence, there is an application dependent optimum condition of these parameters that is required to obtain the maximum thermal performance of PCM slurry flows in microchannels.

To: Lord Sri Venkateswara

ACKNOWLEDGEMENTS

First and foremost, I would like to express my sincere gratitude to my advisor, Dr. Louis Chow for his invaluable guidance and support throughout my dissertation work. I profusely thank him for his patience and knowledge whilst allowing me the room to work in my own way. I attribute the level of my degree to his encouragement and effort and without him this dissertation, too, would not have been completed or written. I could not have imagined a better advisor and mentor for my Ph.D. study.

I would like to thank my committee members Dr. Ranganathan Kumar, Dr. Larry Chew and Dr. Kalpathy Sundaram for their valuable suggestions and especially Dr. Kumar for providing me the license for software use. Special thanks to Dr. Michael Bass for providing additional software license that enabled me to carry multiple simulations simultaneously and speed up the work.

I would like to show my gratitude to the Department of MMAE for providing financial support for my graduate studies at UCF and Dr. Mark Spector, program manager at the Office of Naval Research for funding the research work.

I am highly indebted to all my colleagues and friends who have been with me and helped me in many ways. I highly appreciate the help by all the department personnel who have helped me with travel requests, reimbursements, ordering experiment related stuff and providing computer support etc.

Finally, I wish to thank my parents for their encouragement, patience and moral support.

TABLE OF CONTENTS

LIST OF FIGURES

LIST OF TABLES

LIST OF ACRONYMS

A_b	Area of base, m^2
a	Particle radius, m
B	Width of the channel, diameter of the tube (m)
Bi	Biot number
Bi_p	Biot number of particle
c	Volume concentration of MEPCM particles in slurry
c_m	Mass concentration of MEPCM particles in slurry
$c_{p,b}$	Specific heat of bulk fluid, J/kg.K
$c_{p,f}$	Specific heat of fluid, J/kg.K
$c_{p,p}$	Specific heat of MEPCM particle, J/kg.K
$c_{p,pcm}$	Specific heat of PCM, J/kg.K
D	Hydraulic diameter, m
d_p	Particle diameter, m
e	Magnitude of shear rate, 1/s
f	Enhancement factor
H	Height of the channel, m
H_m	Height of manifold in simulation domain, m
h	Heat transfer coefficient, $W/m^2.K$
h_r	Heat transfer coefficient ratio, $h_{slurry}/h_{base\ fluid}$
h_{sf}	Latent heat of fusion, J/kg
k	Thermal conductivity, W/m.K
k_b	Thermal conductivity of bulk fluid, W/m.K

k_{eff}	Effective thermal conductivity of bulk fluid, W/m.K
k_f	Thermal conductivity of fluid, W/m.K
k_p	Thermal conductivity of MEPCM particle, W/m.K
k_{pcm}	Thermal conductivity of PCM, W/m.K
L	Length of the channel, m
L_{ss}	Length of the channel for fully developed particle distribution profile, m
$\dot{m}$	Mass flow rate inside the microchannel, kg/s
Nu	Nusselt number
n	Unit normal
Pe	Peclet number
PF	$\Delta P_{base\ fluid}/\Delta P_{slurry}$, when $h_{slurry} = h_{base\ fluid}$
Pr	Prandtl number
p	Pressure, psi
p_{in}	Pressure at the inlet, psi
p_{out}	Pressure at the outlet, psi
K_c, K_η	Phenomenological constants
Q	Heat supplied, W
q	Heat flux, W/cm^2
q_w	Constant wall heat flux, W/cm^2
R	Radius (m)
Re	Reynolds number
Re_p	Particle Reynolds number = $Re_{max}(a/H)^2$
R_p	Radius of MEPCM particle, m

$\mathbf{r}$	**S**pace coordinate
r_p	Solid liquid interface radius, m
T	Temperature, K
T_1	Lower melting temperature, K
T_2	Higher melting temperature, K
T_{in}	Temperature at heat sink inlet, K, Temperature at microchannel inlet, K
T_{Mr}	Melting range = T_1-T_2, K
T_m	Melting temperature, K
T_{out}	Temperature at heat sink outlet, K, Temperature at microchannel outlet, K
T_w	Wall temperature, K
$T_{w,max}$	Maximum wall temperature, K
t	Time (s)
t_{base}	Base of microchannel, m
t_{ch}	Half of microchannel width, m
t_{res}	Residence of MEPCM particle inside the channel, s
t_w	Half of Microchannel wall thickness, m
$\boldsymbol{u}, \vec{u}$	Velocity vector, m/s
u	Velocity in x direction, m/s
V_{HS}	Volumetric flow rate at the heat sink inlet, m^3/s
$\mathbf{v}$	Velocity vector
v	Velocity in y direction, m/s
W	Half channel width, m
w	Velocity in z direction, m/s

x,y,z	Spatial coordinates
x	Distance from channel symmetry, m
x	Space vector
ΔP	Pressure drop, psi
ΔP_r	Pressure drop ratio, $\Delta P_{slurry}/\Delta P_{basefluid}$
ΔT_{bulk}	Bulk temperature rise, T_{out}-T_{in}, K
α_p	Thermal diffusivity of MEPCM particle, m^2/s
α_f	Thermal diffusivity of fluid, m^2/s
γ	Shear rate, 1/s
ρ	Density, kg/m^3
ρ_b	Density of bulk fluid, kg/m^3
ρ_f	Density of fluid, kg/m^3
ρ_p	Density of MEPCM particle, kg/m^3
μ	Dynamic viscosity, Pa.s
μ_b	Dynamic viscosity of bulk fluid, Pa.s
μ_f	Dynamic viscosity of fluid, Pa.s
μ_p	Dynamic viscosity of MEPCM particle, Pa.s
p	Pressure (Pa)
Pe	Peclet number

Greek symbols

α	Thermal diffusivity (m^2/s)
γ	Shear rate (1/s)

θ	Non-dimensional temperature = $(T - T_m)/ (q_w R_d/k_{bulk})$
μ,η	Dynamic viscosity (Pa.s)
ν	Kinematic viscosity (m^2/s)
ρ	Density (kg/m^3)
τ	Time constant (s)
φ	Particle volume concentration

Subscripts

b	Bulk
d	Duct
eff	Effective
exit	Exit/Outlet
eq	Equilibrium
f	Fluid
i	Index
inlet	Inlet
l	Liquid phase
m	Mean
max	Maximum
p	Particle
pcm	PCM
s	Solid phase
w	Wall

CHAPTER 1 : INTRODUCTION

Rapid increase in the power densities of ICs and other devices that produce high heat fluxes during their operation demand improvement of available cooling techniques. Tuckerman and Pease in 1981 demonstrated a microchannel heat sink that removes 790W/cm^2 with 71^{0}C temperature increase at 600 mL/min flow rate [1]. Figure 1-1 shows the schematic of a microchannel heat sink. It has numerous small channels and fins arranged in parallel, which are directly fabricated on a silicon substrate and have direct circulation of water. The heat transfer fluid passes from the inlet, picks up heat from the walls along its flow path and exits from the outlet. It is so compact that heat is efficiently carried from the substrate into the coolant because of its inherently small passageways and a very large surface-to-volume ratio. It has already been proved that the use of microchannel heat sinks has numerous advantages compared to macroscale flow channels. Tuckerman and Pease [1] predicted that single-phase forced convective cooling in microchannels should be feasible for circuit power densities of more than 1000 W/cm^2. However, the heat sink had quite large pressure drop of 200kPa with plain microchannels and 380kPa with pin fin enhanced microchannels. For single phase cooling, the coolant temperature will increase in the flow direction as it acquires heat, which leads to non-uniform temperature distribution on the chips. In order to keep the temperature of devices such as semiconductors and lasers to be cooled within a few degrees Celsius, a very large mass flow rate is needed, resulting in high pressure drop across the microchannels and requires a large pump.

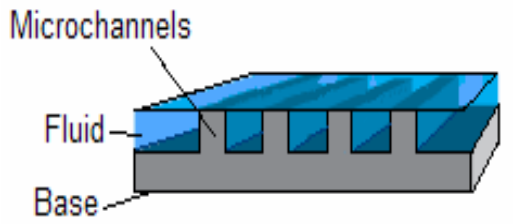

Figure 1-1. Traditional microchannel heat sink

One of the factors that influence the temperature variation is the specific heat capacity of the coolant. For a constant heat input Q, the temperature difference between the inlet and outlet of each channel can be given as

$$\Delta T_{bulk} = \frac{Q}{\dot{m} c_p} \tag{1.1}$$

As can be seen from the equation, the temperature difference can be reduced by increasing the mass flow rate or the specific heat capacity of the coolant. Traditional microchannels even though showed substantial improvement in the cooling performance, they have two main disadvantages: the relatively high pressure loss and significant temperature variation within the heat source.

1.1 Manifold Microchannel (MMC) Heat Sinks

An MMC heat sink, on the other hand, has the coolant flowing through alternating inlet and outlet manifolds in the direction normal to the heat sink base. Figure 1-2 shows the geometry and flow domain inside single microchannel. The flow path is greatly reduced to a small fraction of the total length of the heat sink thus reducing the resultant pressure drop and restraining the length of the thermal boundary length along the streamwise direction.

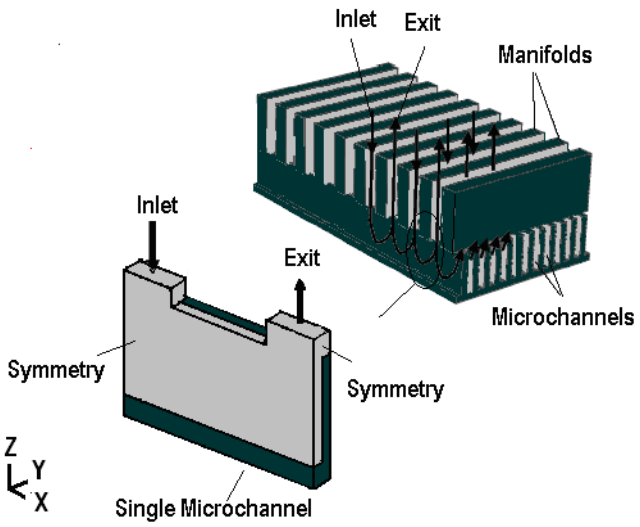

Figure 1-2. MMC heat sink flow path and flow domain

Harpole and Eninger [2] proposed and MMC system having between 10 and 30 manifold channels and reported that for constant flow rate or pumping power, the maximum temperature and temperature variation within the heat source were substantially reduced from that of a TMC heat sink. Copeland et al. [3] tested a variety of MMCs experimentally and reported that the thermal resistance was inversely proportional to the volume flow rate on a log–log scale.

Copeland et al. [4] showed that the simple analytical model based on correlations for straight channels is not satisfactory for predicting the performance.

In order to increase the effective specific heat of the fluid, boiling heat transfer inside microchannels has been investigated to utilize latent heat of vaporization [5]. However, the increased pressure drop and associated pressure fluctuation, and wall temperature fluctuation in minichannels and microchannels hinder the application of convective boiling in microchannels for electronic cooling. Possible dry-out at relative low heat flux compared with its single flow counterpart prevents two-phase flow in microchannels to be used in cooling of high heat flux components/electronics [6]. One other way of increasing the heat capacity of the fluid is to use phase change materials inside the fluid as described in the next section.

1.2 Encapsulated Phase Change Material (EPCM) Slurry

In the last two decades, the use of phase change material in thermal control systems and thermal energy storage has been proposed. A solid-liquid phase change material (PCM) is any material, which absorbs heat when it melts and releases that heat when it solidifies. This phase change enables the PCM to act as heat storage media. Most of the available researches show that PCMs have been microencapsulated and suspended in a heat transfer fluid to create a phase change slurry or MEPCM slurry (Figure 1-3). MEPCM particles consist of PCM encapsulated in a shell so that they remain separate from carrier fluid. Figure 1-4 shows the SEM image of MEPCM particles. These particles can be as small as 1 μm to as high as 500 μm. The shell of the particle is usually thinner compared to particle diameter.

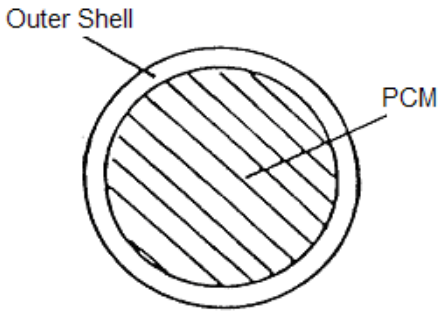

Figure 1-3. Cross section schematic of a single MEPCM

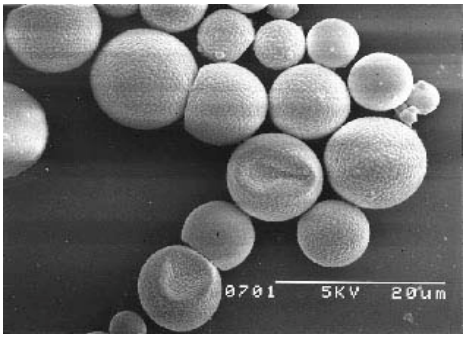

Figure 1-4. Scanning electron microscope of microencapsulated PCM particles

NEPCM slurry is a two-phase fluid with a base fluid and nanosized particles. A sample of nanosized PCM particle slurry was made at University of Central Florida with water as base fluid and Octadecane as PCM. The particle size is around 100nm and the shell thickness is around 5 nm. It is prepared by emulsification process where a surfactant (shell material) is first dissolved in the base fluid and is then heated to a temperature greater than the melting point of PCM while stirring continuously. Later the PCM is added to the mixture to carry out the emulsification. The formation of the nanoPCM was confirmed using the Tyndall's effect. This involves the scattering of a laser beam as it passes through the emulsion due to the presence of

nano-sized particles. Pure water itself cannot scatter the laser beam. Figure 1-5 shows the measured size distribution of the sample with a diameter distribution at around 60 nm to 125 nm.

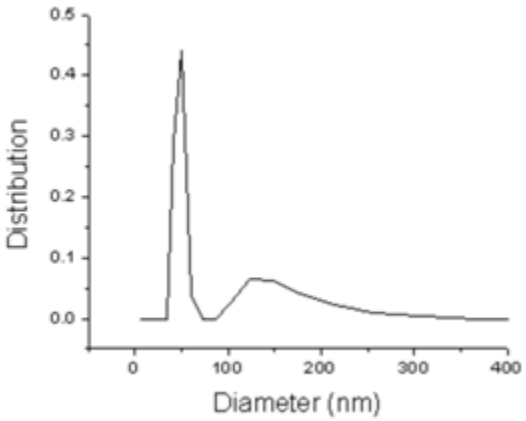

Figure 1-5. Size distribution of NEPCM particles in slurry sample

Figure 1-6 shows the Differential Scanning Calorimetry (DSC) curve of the NEPCM sample. For the DSC measurement, 5 mg of the sample was heated at a rate of 2 ^{0}C/min. A slightly broader peak at around 20 ^{0}C is due to the phase change of PCM. It can be observed that the phase change peak is around 20 ^{0}C and not between 28 ^{0}C to 30 ^{0}C, typical to Octadecane which is probably induced by the small size at nanoscale, where the surface effect is much more significant than that at micro scale. The estimated latent heat of the PCM has a high degree of uncertainity and was found to be between 100 kJ/kg and 240 kJ/kg.

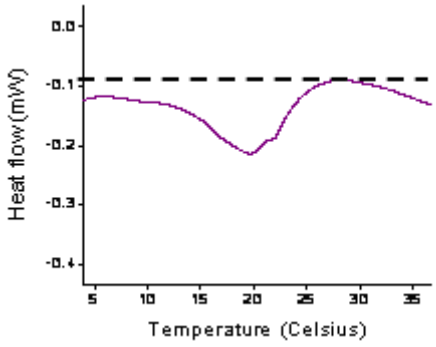

Figure 1-6. DSC curve of NEPCM slurry

EPCM particles when mixed in a fluid increase the heat capacity of the fluid during phase change. The slurry can be considered as two-component Newtonian fluid for concentrations up to 0.3 [7], with the effective specific heat during phase change given by [8]

$$c_{p,eff} = \bar{c}_p + \frac{x c_m h_{sf}}{\Delta T_{bulk}} \tag{1.2}$$

where $\bar{c}_p$ is the weighted average specific heat given by $\bar{c}_p = (1 - c_m)c_{pwf} + c_m c_{pcm}$, x is the fraction of particles undergoing phase change, c_m is the loading fraction, ΔT is the temperature rise of fluid, h_{sf} is the latent heat of melting of PCM, c_{pwf} is the specific heat of working fluid and c_{pcm} is the specific heat of solid PCM. As an example, assuming the PCM has completely change its phase from solid to liquid at the exit of channels (x=1), working fluid as water, the loading fraction is 0.2, latent heat of PCM as 250kJ/kg, c_{pcm} as 2 kJ/kgK and ΔT as 3^oC, the effective specific heat will be 21 kJ/kg.K. This implies that the specific heat is increased by about 5 times with the presence of MEPCM during melting.

As a heat transfer working fluid, EPCM slurries lie between sensible fluids and fully latent fluids. The fluid possess the desired control, flow, and predictability characteristics of simple liquids, while also having the enhanced thermal capacitance and heat transfer characteristics of phase-change fluids. EPCM fluids possess many attractive features such as high-energy storage density, high heat transfer rates between wall and suspension and low pumping power requirements. Experiments showed that microcapsules with diameter in the range of 5 μm to 50 μm can be pumped and circulated without any significant damage [9, 10]. There are no experiments with NEPCM slurry as heat transfer fluid. It can be assumed that nanosized particles also can be pumped without any significant damage, as there will be not be significant shear on the particles due to the flow as will be explained in Chapter 4.

Compared to single-phase fluids, the advantages of PCM slurry can be summarized as:

- Store higher quantities of heat per mass unit.
- Store heat at temperatures where the heat losses to ambient are low.
- Deliver more heat at same mass flow rate.
- Increase the heat capacity of a water based heating or cooling application by refilling the system with phase change slurry.

The performance of fluid in microchannels can be different compared to performance in conventional channels owing to the small size. Numerical simulation of slurry flow in microchannels helps in understanding and assessing the useful parameters that affect the flow and thermal performance of EPCM slurry. The present work focuses on understanding the role of particle diameter, particle concentration, particle distribution and fluid properties in predicting the thermal performance of slurry in microchannels. It will also provide useful information to

develop new models for designing future thermal systems that use EPCM slurry flow in microchannels.

CHAPTER 2 : LITERATURE REVIEW

The EPCM slurries provide greater heat transfer and possess high specific heats only during phase change. The heat transfer phenomenon of slurry flows is not fully understood. Properties like specific heat, conductivity and other thermodynamic properties of the slurry depend on the phase change of particles and complicate the heat transfer analysis. Because of this complexity, the theoretical and experimental investigations of a slurry flow with phase change are very difficult [7-33].

In a prototype solar collector pump system, Hart and Thompson [9] tested a slurry of 30% wax in oil. From the results, they concluded that at a temperature between 311 and 322 K, the effective specific heat was around two times greater than the pure oil. McMahon et al. [10] carried out thermal performance tests of slurries (n-heptadecane and n-Octadecane in ethylene glycol) as cooling fluids for protective garments and reported a specific heat increase of 20 percent. Colvin and Mulligan [12] investigated the application of phase change as a heat transfer fluid and thermal storage medium in spacecraft, electronic systems, and avionics. They reported an enhanced specific heat up to 5 times higher than that of pure fluid at temperature difference of 2 ^{0}C and a heat transfer coefficient of about 2.8 higher than water. Heat transfer enhancement in the flow of suspensions has been reported by many investigators [13, 34-35]. Results of experiments in [34, 35] showed the effective conductivity of about 10 to 80 times higher than that of the pure fluid, depending on the velocity gradient at the wall and the particle/duct ratio. The heat transfer enhancement phenomena were analyzed and correlations for effective thermal conductivity were derived [36-38]. Thus, phase change slurries can also benefit from increased heat transfer enhancement due to the presence of particles.

Chen and Chen [13] investigated the heat transfer augmentation for a steady, laminar phase change slurry flow above a flat plate with constant wall temperature. They found that the convective heat transfer rate is proportional to the square root of Reynolds number and the Prandtl number to the $1/3^{rd}$ power and inversely proportional to the cube root of the Jacob number multiplied by the mass fraction of the phase change material. No further details or comparisons were provided.

Charunyakorn et al. [7] developed a numerical model for encapsulated phase change suspension flow between parallel plates for different boundary conditions for low temperature applications. They also obtained numerical solutions for MEPCM suspension flow in circular tubes with boundary conditions of constant heat flux and constant wall temperature. Their results showed that the volumetric concentration and the bulk Stefan number are the important parameters that influence the heat transfer process. Goel et al. [16] conducted an experiment using n-eicosane microcapsules in water for laminar, hydrodynamically fully-developed flow in a circular tube with a constant heat flux boundary condition. The wall temperature could be reduced up to 50% by using a PCM suspension instead of a single phase fluid for the same dimensionless parameter in their experiments. Though their results agreed qualitatively with that of predictions by Charunyakorn et al., there was a quantitative difference greater than 45% between them.

Zhang and Faghri [18] presented a numerical solution of laminar forced convection of a microencapsulated phase change material suspension in a circular tube with constant heat flux. Instead of using the quasi-steady model employed by Charunyakorn et al. [7], they used a temperature transforming model to solve the problem and considered the effects of

microcapsule's crust, and the initial subcooling. Their numerical predictions differ from the experimental results [16] quantitatively by 34%. Their results showed that the effect of microencapsulated PCM on the forced convection heat transfer reduces as the melting temperature range increases. However, they concluded that it is necessary to determine the extent of the phase change temperature range by further experimental work.

Alisetti and Roy [31] have simulated the steady, laminar MEPCM slurry flow inside a tube with constant wall temperature boundary condition. They have modeled the slurry flow as a single phase fluid with varying effective specific heat. Their results showed that the dominant parameters are the bulk Stefan number, the degree of subcooling, and the dimensionless melting temperature range and the effect of the specific heat ratio is very small in the range of parameters considered.

Hao and Tao [23], and Xing et al. [24] have developed a model for simulation of the laminar hydrodynamic and heat transfer characteristics of suspension flow with micro-nano-size phase change material particles in a microchannel. Their results demonstrate the sensitivity of the temperature distribution inside the tube with the initial fluid temperature.

Hu and Zhang [33] used an effective specific heat capacity model to analyze the heat transfer enhancement mechanism of a functional thermal fluid for sensitivity analyses of some major factors that influence the heat transfer enhancement in circular tube with constant heat flux. Zhang et al. [22] used the specific heat capacity model to analyze the effect of the phase change and the effective thermal conductivity on the heat transfer enhancement of MEPCM slurries for laminar flow in a circular tube with constant wall temperature.

Rao et al. [26] conducted heat transfer experiments with MEPCM slurry in mini channels with water as base fluid and n-Octadecane as PCM. They found that slurry was not always better compared to the pure fluid. They mentioned that this could be because of decrease in thermal conductivity of slurry compared to water.

Recently, Sabbah et al. [32] have numerically studied the thermal performance of PCM slurry in traditional microchannels. They used water as base fluid and Octadecane as PCM. They mentioned that inclusion of wall in numerical modeling is important.

2.1 Scope of the Work

While all preliminary studies and experiments indicate promising applications of phase change slurry as a heat transfer fluid, there have been no considerable studies of PCM slurry in microchannels. Most of the studies were conducted for conventional channels and tubes. Compared to the flow in macrochannels, the heat transfer enhancement in microchannels is large due to the presence of walls. Hence, the inclusion of fin or wall effect of microchannels is important to include while simulating flow inside microchannels.

Models by Charunyakorn et al. [7], Zhang and Faghri [18], use a sink term in their model to account for the presence of PCM. Charunyakorn's model neglects the particle wall and uses a quasi-steady model to calculate the amount of heat absorbed by PCM particle. Moreover, they assumed that the suspension enters the tube exactly at the melting point and the all the melting occurs exactly at the melting point of PCM. This is not a realistic assumption, as there is a

melting range for PCMs in reality due to the supercooling of PCM (for example, salt hydrates), impurities (paraffins) etc.

Zhang and Faghri's model includes the melting delay inside the particle, and includes the particle wall. All three models [7, 18, 31] assume laminar and hydrodynamically fully developed flow in macrochannels. They have assumed homogeneous distribution of particles, which may not be true when the duct to particle diameter ratio is smaller as in case of microchannels.

The model followed in [23, 24] does not consider the wall effects. Moreover, the microchannel was considered as a tube which is not the actual case. The model uses the fluidized bed correlations to solve the particle distribution and is derived for two-dimensional cylindrical flows. They mentioned that including the particle distribution in the numerical model predicts the temperature distribution equally or more accurate than the temperature distribution predicted by models that assume homogeneous particle distribution. Model used by Sabbah et al. [32] considered the three dimensional fin effects in microchannels, but the effect of particle distribution inside the microchannel was not considered. In addition, only a few parameters like microchannel wall, heat flux and particle concentration were varied in their model.

From the above discussion, it can be concluded that little work was done on investigating the EPCM slurry characteristics in microchannels. The effect of particle distribution in micorchannels was not investigated. In addition, when the microchannel lengths are short like in MMC heat sinks (key focus of the present study), the performance of slurry might be different. Hence, the current work focuses on the following specific tasks:

i. To simulate the particle distribution inside the microchannels and study its effect on the overall performance of microchannel heat sinks compared to single phase fluids.

ii. To study the performance of slurry in more detail by varying the slurry and thermal parameters.

iii. To compare the numerical model results with experimental work and obtain solutions that may be used as a basis for preliminary work or a guideline in planning when PCM slurries are employed.

For investigating the particle migration effect, a macroscopic model based on shear-induced migration was used for solving the particle migration inside the channel. The calculated particle concentration profile was then used to analyze the thermal performance. The parametric study in the current work investigated the importance of PCM melting range, particle mass concentration, inlet temperature, base heat flux, channel dimensions and base fluid.

CHAPTER 3 : PARTICLE DISTRIBUTION INSIDE MICROCHANNELS

When slurry or a suspension flows inside a channel, the particles tend to migrate and the flow becomes nonhomogeneous even though it is homogeneous at the inlet. The mechanisms suggested for particle migration in concentrated suspensions include hydrodynamic interactions, electrostatic interaction, and other surface interactions that become important as the particles are close. The development of particle migration profile depends on several parameters as described in next section.

3.1 Particle Migration inside a Channel

Migration of particles in a tube has been first observed by Siegre and Silberberg [39] and noted that a neutrally buoyant particle tends to migrate to an equilibrium position approximately at 0.6r, at low Re, where r is the pipe radius. This effect is known as Siegre and Silberberg effect or tubular pinch effect (Figure 3-1).

The migration of a particle inside a channel can be attributed to different forces. In cases where Brownian motion is negligible, the migration of particles has been attributed to the presence of inertial forces. However, under vanishingly small particle Reynolds numbers, inertial forces are not dominant and the migration of particles depends purely on the shear-induced forces. Most studies on particle migration in semi-concentrated or concentrated suspensions have been focused on the cases of vanishingly small particle Reynolds number, Re_p [40-49]. These models are based on different simulation techniques such as Stokesian dynamics, Lattice

Boltzmann methods, dissipative particle dynamics and the Lagrange multiplier fictitious domain method.

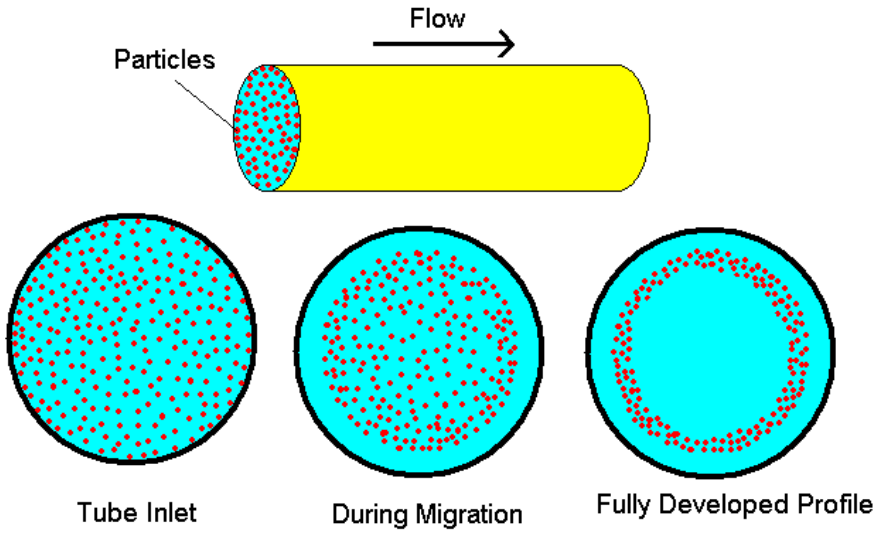

Figure 3-1. Particle distribution over a cross section of tube

At the length scale of the particles, the mechanics of suspension systems are governed by the Navier-Stokes equations. Microscopic methods and lattice Boltzmann methods can provide valuable insight to many body interactions. Solutions could theoretically be found for each particle, but due to the multibody interactions, the mathematics becomes complicated with even just a few. However, the number of particles explicitly modeled in these simulations is currently limited to the order of several thousand using high-end computers because of the large CPU and memory requirements. It is reasonable to consider the suspension as a continuum for most applications because many suspended particles are less than a few micrometers in diameter. From a practical point of view, a macroscopic constitutive equation is preferable, as it allows the modeling of realistic macroscopic problems which contain extremely large number of suspended

particles. Several constitutive models have been put forth recently which basically fall into two categories. One category comprises of models based on conservation of mass and momentum for suspension components [43], the other category comprises models based on shear-induced particle migration and diffusion [42, 49].

The second category models, collectively referred as diffusive flux model (DFM) are based on the scaling arguments proposed in [42]. Leighton and Acrivos [42] suggested phenomenological models for particle migration in nonhomogeneous shear flow typically due to spatial variation in irreversible interaction frequency and effective viscosity. Phillips *et al* [49] adapted the scaling arguments of Leighton and Acrivos, and proposed a diffusive-flux equation to describe the time evolution of the particle concentration based on the two-body interactions. For analyzing the particle distribution inside the microchannel for the current work, the DFM proposed by Philips et al. [49] was used.

3.2 Diffusive Flux Model (DFM)

The method proposed by Philips et al. [49] as applied to a three-dimensional rectangular duct can be summarized as follows. The shear-induced migration of particles is the result of shear rate gradients and the concentration gradients. The particle flux based on the phenomenological model is given by:

$$J = -K_c a^2 \phi \nabla(\phi \dot{\gamma}) - K_\eta a^2 \frac{\phi^2}{\eta} \nabla \eta \tag{3.1}$$

K_c and K_η are the phenomenological constants that must be determined by fitting the predictions of the model and the experimental results. These values for both 2-D tube and channels flows were predicted as 0.62 and 0.41 [49]. The dynamics change of particle concentration along the flow is governed by the particle balance:

$$\frac{D\phi}{Dt} = \nabla . J \tag{3.2}$$

With the assumptions mentioned above, the mass and momentum equations for the phase change slurry can be written as:

$$\nabla . \vec{u} = 0 \tag{3.3}$$

$$\nabla . \left[\eta (\nabla \vec{u} + \nabla \vec{u}^T) \right] - \nabla p = 0 \tag{3.4}$$

The effective viscosity of a concentrated suspension can be given by the Krieger's formula [50]:

$$\eta = \eta_f \left(1 - \frac{\phi}{\phi_m} \right)^{-m} \tag{3.5}$$

where, the maximum concentration can be 0.6 to 0.68 and the empirical m is equal to 1.82. Diffusive flux model is valid for slow flows and it can be used for particle Reynolds numbers less than 0.1 [51]. K_c and K_η are the phenomenological constants that must be determined by fitting the predictions of the model and the experimental results.

3.2.1 Boundary conditions for flow and particle distribution

For particle distribution, the following boundary conditions are used

$$\phi = \phi_0 \text{ , at the inlet} \tag{3.6}$$

$$[\eta(\nabla u + \nabla u^T)].n = 0 \quad p = p_0 \text{ , particle outlet} \tag{3.7}$$

$$n.[K_c \phi \nabla(\dot{\gamma}\phi) + K_\eta(\dot{\gamma}\phi^2)\frac{1}{\eta}\frac{\partial \eta}{\partial \phi}\nabla\phi] = 0 \text{ , the total flux at the wall and the symmetric boundary is zero.} \tag{3.8}$$

3.2.1.1 Developing length of particle distribution

Particle distribution can be considered to achieve the equilibrium position if there is no change in the particle profile. Nott and Brady [43] analyzed the time scale for particles to reach steady state based on the shear-induced-diffusion hypothesis [42] and is given by:

$$t_{ss} \sim \left(\frac{2W}{a}\right)^3 \frac{a}{12d(\phi) < u >} \tag{3.9}$$

where, W is half of the channel width, a is the particle radius, <u> is the average velocity. For dense suspensions, (φ>0.3), 12d(φ)~1. Hence, the length along the channel required to achieve steady state is given by:

$$\frac{L_{ss}}{2W} \sim \frac{1}{12d(\phi)}\left(\frac{2W}{a}\right)^2 \tag{3.10}$$

This length is the characteristic length scale for the process and it requires several transition lengths before the final equilibrium state is reached. Experiments by Hampton et al. [52] shows a range of values for the exponent n, increasing linearly from 0.4 for φ = 0.2 to 1.8 for φ = 0.45. Authors in [53] found that the value of n is around 1 for particle concentration of 0.24 and around 2 for particle concentration of 0.35. Assuming H = 100 μm, a = 2.5 μm and particle concentration is 0.3, which is between 0.24 and 0.35, particle steady state profile can be achieved between a length of 4 cm and 16 cm. It can be observed the migration development length is very long compared to the usual length of MMC heat sinks, which is around 1 mm. Hence, the effect of particle migration on thermal performance was investigated in traditional microchannel heat sinks.

For the present study, the particle distribution is modeled in microchannels of large aspect ratio (>=10), where the flow can be considered to be two-dimensional. This was done in order to use the readily available 2-D values for K_c and K_η. This is justifiable since the main aim of this work is to look at the thermal performance of nonhomogeneous slurry in a microchannel.

3.2.2 Assumptions for thermal simulation

For solving the temperature of slurry, the problem was formulated based on the following assumptions.

i. The slurry properties are function of particle concentration. Segre and Silberberg [39] found that the radial migration of the particles is a function of 2.84^{th} power of particle/duct diameter ratio. When the duct or channel size is very small like in the case of microchannel, the ratio can be large.

ii. The specific heat capacity of the fluid is a function of temperature. The slurry thermal conductivity is a function of the particle Peclet number and varies across the flow field.

iii. The melting inside EPCM particles takes place over a range of temperatures, between T_1 and T_2 with the peak melting point at a temperature, T_m.

iv. There is no temperature gradient inside the particle or the particle melts instantaneously. This assumption has been discussed in later sections. The particle sizes, where this assumption is valid will be considered for simulation.

v. The effect of particle depletion layer is negligible. The particle depletion layer is of the order of the particle radius if the channel size to particle size is large [54, 55].

vi. The shape of the encapsulated particles is spherical. The shell material is very thin and hence the particles are considered to consist totally of the phase change material.

3.2.2.1 Validation of assumptions for thermal simulation

- Assumption iv: Particle melts instantaneously

Since the length of the channel is short for the MMC channel, it is important that the PCM particle completely melts within its residence time. Charunyakorn et al. [7] applied the method proposed by Tao [56] to calculate solid-liquid or melt interface r_p (Figure 3-2) in a sphere for calculating the source term in their model.

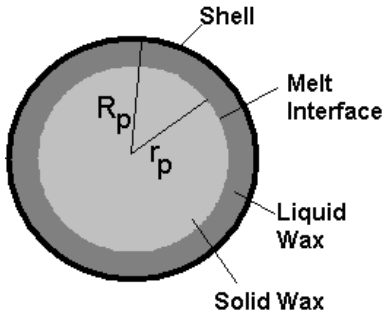

Figure 3-2: Particle melting process

Assuming the particle has to melt 99% by the time it exits the channel, the required temperature difference between the surrounding fluid T_f and the melting temperature T_m, of the PCM was calculated (Equation 3.11) using the same analogy.

$$T_{fm} = T_f - T_m = \left[\frac{1}{2}\left[1 - \left(\frac{r_p}{R_p} \right)^2 \right] + \frac{1}{3}\left[1 - \left(\frac{r_p}{R_p} \right)^3 \right] \left(\frac{1}{Bi_p} - 1 \right) \right] . \frac{h_{sf} . R_p^{\,2}}{t . \alpha_p . c_p} \tag{3.11}$$

where, the Biot number of the particle is given by [56]:

$$Bi_p = \frac{k_{eff}}{k_{pcm}} . \frac{2(1-c)}{2 - 3c^{\frac{1}{3}} + c} \tag{3.12}$$

Figures 3-3 and 3-4 show the required temperature difference between the fluid and the particle melting temperature with water and PAO as base fluids in a channel of 100 μm width and 1 cm length for different Re. It can be observed that the required T_{fm} increases with the increase in particle radius. It can be observed that the particle may not completely melt if the channel length is short. For calculations, properties in Table 3-1 were used.

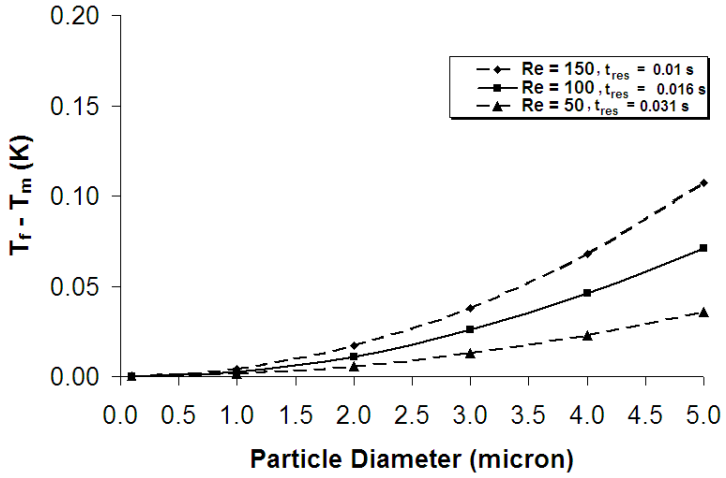

Figure 3-3. $T_f - T_m$ for different particle diameters (base fluid - water)

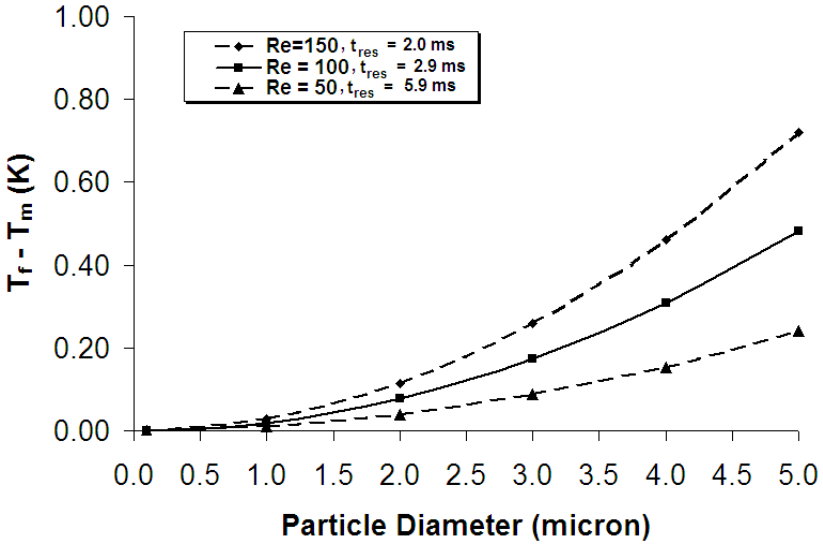

Figure 3-4. $T_f - T_m$ for different particle diameters (base fluid - PAO)

Table 3-1. Thermophysical properties used in Figures 3-3 and 3-4

	Density (kg/m^3)	Specific heat (J/kg.K)	Thermal conductivity (W/m.K)	Viscosity (kg/m.s)	Latent heat (J/kg)
PAO	783	2242	0.143	$4.45x10^{-3}$	-
n-Octadecane	815	2000	0.18	-	$244x10^3$
Water	997	4180	0.604	$1x10^{-3}$	-

3.2.3 Governing equations for thermal simulations

After the particle distribution is solved using the DFM, the thermal performance of slurry was modeled assuming slurry as a bulk fluid with varying properties which are a function of particle concentration. The energy equation for the slurry and the boundary conditions are:

$$\rho c_p\left(u\frac{\partial T}{\partial x}+v\frac{\partial T}{\partial y}\right)=\frac{\partial}{\partial x}\left(k\frac{\partial T}{\partial x}\right)+\frac{\partial}{\partial y}\left(k\frac{\partial T}{\partial y}\right) \tag{3.13}$$

$$T = T_{in} \quad \text{at the inlet for fluid} \tag{3.14}$$

$q.n = (\rho c_p \mathbf{u} T).n$; which is the convective heat flux boundary condition at the outlet/exit (3.15)

$$q.n = q_w; \text{ constant heat flux at the wall} \tag{3.16}$$

$$q.n = 0; \text{ insulation at the symmetry or channel half-width} \tag{3.17}$$

3.2.3.1 Effective thermal conductivity

Slurry thermal conductivity and specific heat is defined follows. For dilute suspensions of static bulk fluids, thermal conductivity of the suspension can be defined as for conductivity in a medium with distributed spherical particles [57]:

$$k_b = k_f . \frac{2 + \frac{k_p}{k_f} + 2c(\frac{k_p}{k_f} - 1)}{2 + \frac{k_p}{k_f} - c(\frac{k_p}{k_f} - 1)} \tag{3.18}$$

Yamada and Takahashi [58] investigated experimentally the thermal conductivity of suspensions of particles of different shapes. They found an excellent agreement between their experimental values for suspensions of spherical particles. The results for other shapes compare less favorably. For flowing slurries, the effective thermal conductivity is higher than that calculated by Equation 3.18 due to diffusion related enhancements. For dilute suspensions, it can be evaluated as follows [7]:

$$k_{eff} = f . k_b \tag{3.19}$$

$$\begin{cases} f = 1 + BcPe_p^m \\ B = 0, \quad m = 1.5, \quad Pe_p < 0.67 \\ B = 1.8 \quad m = 0.18 \quad 0.67 \le Pe_p \le 250 \\ B = 3.0, \quad m = \frac{1}{11}, \quad Pe_p > 250 \end{cases}$$

The particle Peclet number is defined as,

$$Pe_p = \frac{ed_p^{\,2}}{\alpha_f} \tag{3.20}$$

Since the velocity is not fully developed in the current analysis, the shear rate is a function of all the spatial coordinates and corresponding velocities. The magnitude of the shear rate, *e* can be calculated using the following equation.

$$e = \left(\frac{1}{2} \sum_i \sum_j \gamma_{ij} \gamma_{ji} \right)^{1/2} \tag{3.21}$$

γ is the shear rate.

3.2.3.2 Effective density

For slurries, the density can be calculated by the weighted mean method given in Equation 3.22 [7]. The mean density ρ_m is the average of the densities of PCM solid and liquid phases.

$$\rho_b = c\rho_m + (1-c)\rho_f \tag{3.22}$$

3.2.3.3 Effective specific heat

The phase change inside the particles can be modeled using latent heat method or effective specific heat capacity method. Latent heat method can be used to model pure PCMs where as the effective specific heat method can model the melting range of PCMs easily. Alisetti and Roy [31] have used various profiles for the specific heat of PCM for calculating the effective specific heat and have shown that the difference between the solutions is less than 4%. When PCMs are encapsulated, due to the nucleation, there usually is a melting range for the PCMs, and this increases with decrease in particle size. Of all the different profiles, sine profile (Figure 3-5) has been used to represent EPCM particle specific heat. This was done in order to avoid sudden variation in the property and thus help in reducing the convergence problems. As there is not much variation, the specific heat of solid and liquid phases of PCM was assumed to be equal.

$$c_{p,p} = c_{p,pcm} + \left\{ \frac{\pi}{2} . \left(\frac{h_{sf}}{T_{Mr}} - c_{p,pcm} \right) . \sin \pi \left[\frac{(T - T_1)}{T_{Mr}} \right] \right\} \tag{3.23}$$

The effective specific heat of the slurry can be calculated as:

$$c_{p,b} = c_m c_{p,p} + (1 - c_m) c_{p,f} \tag{3.24}$$

The value specific heat of the particle in Equation 3.24 is equal to $c_{p,pcm}$ when the temperature of the particle is outside the melting range and is given by Equation 3.23, when the particle temperature is within the melting range.

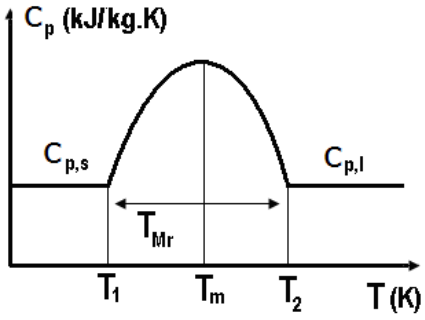

Figure 3-5. Specific heat of EPCM, function of temperature

3.3 Particle Distribution Results

The microchannel dimensions used for simulation of particle distribution are 100 μm width, 1mm height and 1 cm length. As mentioned before, the simulation domain can be considered 2D for such high aspect ratios. Commercial FEM software, COMSOL was used for all the numerical simulations in the dissertation work [59]. Following parameters were varied.

i. Base fluid: Two different fluids were used, water and poly-alpha-olefin (PAO). PAO is a dielectric fluid used for cooling of military avionics applications. It is a stable and inexpensive fluid.

ii. Particle diameter: 100nm, 1 μm, 5 μm

iii. Particle concentration: 0.05, 0.1, 0.3

iv. Channel Reynolds number: Since DFM is valid for Re_p<=0.1, it was found that the maximum Reynolds number of the fluid that can be modeled was calculated using the following calculation:

$$Re_p = Re_{max}(a/H)^2 \tag{3.25}$$

For current simulation, a = 2.5 μm, H = 100 μm. Substituting the value of Re_p = 0.1, $Re_{max.}$ is 160. Thus three different channel average Reynolds numbers were used for simulating the particle migration. Table 3-2 below shows the inlet velocities when water and PAO were used.

Table 3-2. Re values used for simulating particle migration

Channel Re_{avg}	**V_{in}, Water**	**V_{in}, PAO**
80	0.357 m/s	2.276 m/s
60	0.268 m/s	1.707 m/s
30	0.134 m/s	0.850 m/s

For the above calculations, the density and viscosity of pure fluid must be used. The values are used from Table 3-1.

3.3.1 Effect particle diameter on particle migration

Figure 3-6 shows the particle distribution at a length of 1 cm for all the three particle diameters used with PAO as base fluid. The particle mass concentration is 0.3 and Re_{avg} is 80. It can be observed that the migration is highest for 5 μm diameter particle and there is no migration for 100 nm particle size.

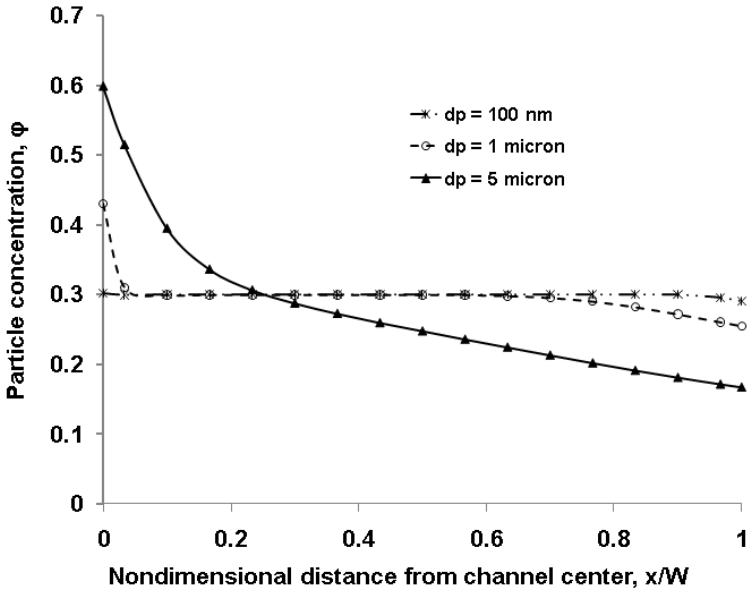

Figure 3-6. Particle distribution with varying particle diameter (base fluid - PAO)

3.3.2 Effect of particle volume concentration on particle migration

Figure 3-7 shows the particle migration at a length of 1 cm from the inlet for a particle diameter of 5 μm and Re_{avg} of 80. It can be observed that the migration is high when the particle mass concentration is higher.

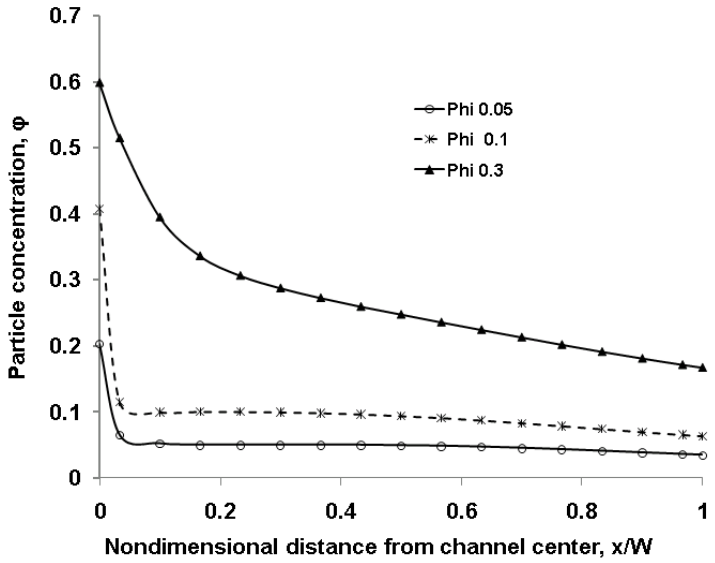

Figure 3-7. Particle distribution as a function of concentration (base fluid - PAO)

3.3.3 Effect of inlet velocity on particle migration

Simulations with three different Re_{avg} were run and it was found that there was no effect of inlet velocity on particle migration. Figure 3-8 shows the particle concentration profile obtained with water based slurry for all three Re_{avg}. This type of result was also obtained in [52]. The reason could be that the diffusive flux model does not include the inertial forces and hence the variation in velocity does not effect the particle migration. The variation in concentration

profile was only dependent on the a/H ratio, i.e., the particle radius to the tube radius or channel width.

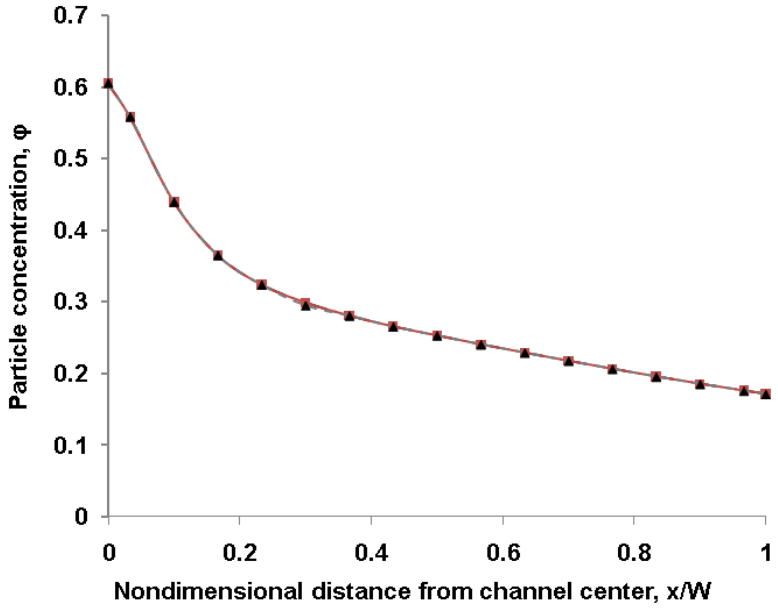

Figure 3-8. Particle distribution profile, base fluid-water

3.3.4 Particle migration along the length of the channel

It is interesting to observe the transformation of homogeneous profile into nonhomogeneous along the length of the channel. Figure 3-9 shows the particle distributions at different lengths from inlet for PAO. The Re_{avg} used is 80 and particle concentration is 0.3. It can be observed that the particle migration rate increases with increase in length.

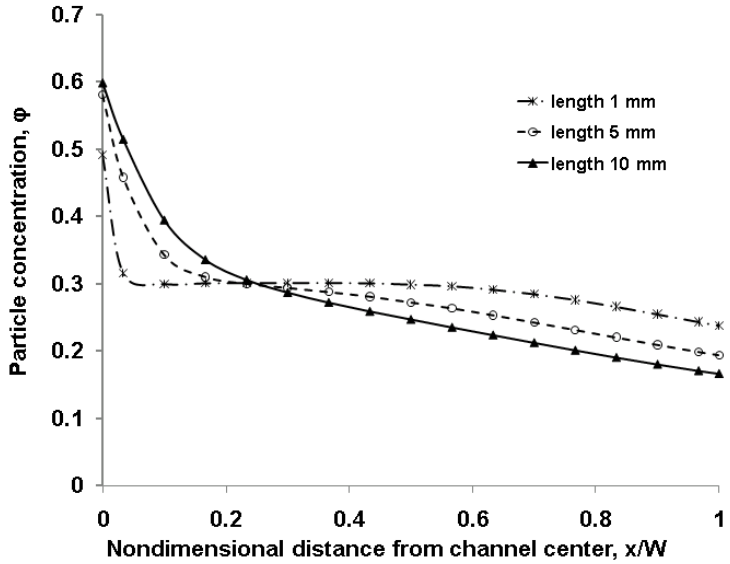

Figure 3-9. Particle concentration at different locations along length (PAO)

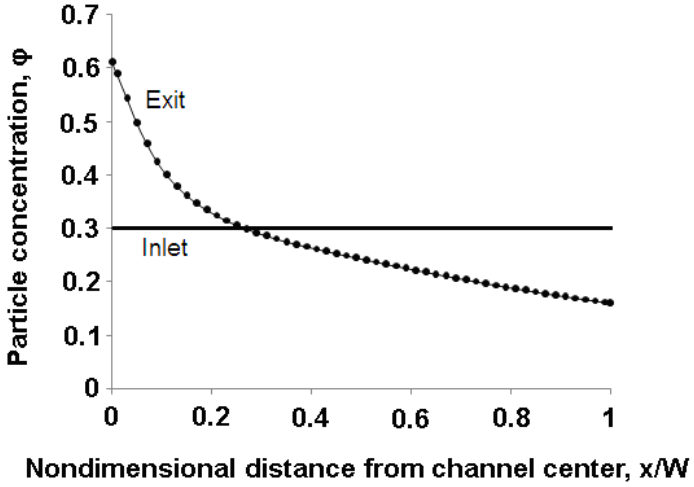

Figure 3-10. Particle concentration profile for developing assumption

3.4 Thermal Performance Results

The effect of particle migration on thermal performance was investigated by comparing the thermal results obtained assuming the particle profile is developing (uniform profile at inlet

and nonuniform profile at the exit as shown in Figure 3-10) and the results obtained assuming the particle profile is homogenous (uniform at both inlet and exit as shown in Figure 3-11).

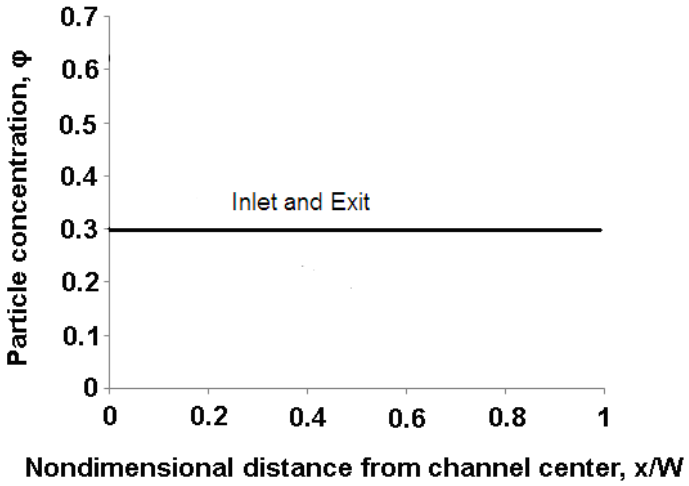

Figure 3-11. Particle concentration profile for homogeneous assumption

The particle distribution obtained for a particle diameter of 5 μm and particle concentration of 0.3 was used for thermal simulations as maximum migration was observed at these conditions. Figures 3-12 and 3-13 show the difference in maximum wall temperature and the inlet temperature for both fluids. The average Re used was 80 and a melting range of 6 K was used. PCM melting peak was assumed to be at 27 ^{0}C. The difference in wall temperature for both assumptions is not more than 1.4 K for water and is 1 K for PAO.

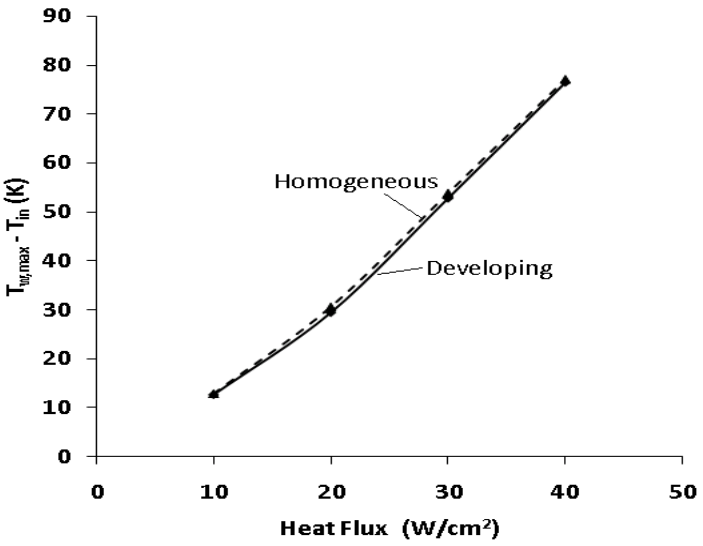

Figure 3-12. Difference in maximum wall temperature and inlet temperature for both assumptions (base fluid - water)

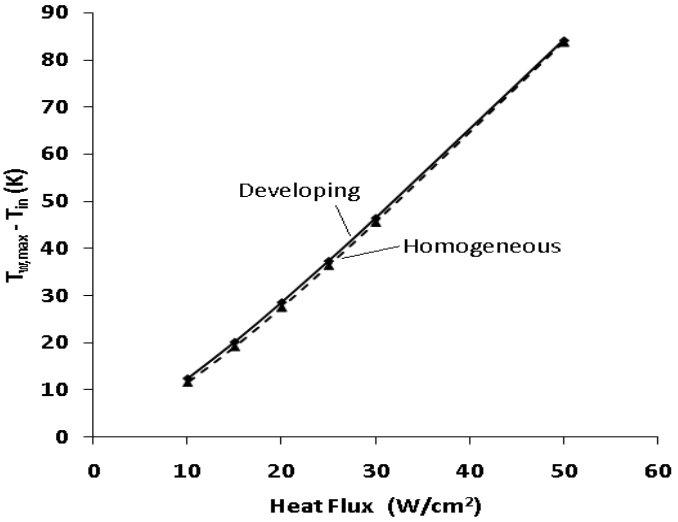

Figure 3-13. Difference in maximum wall temperature and inlet temperature for both assumptions (base fluid - PAO)

3.4.1 Analysis of the results

From previous results, it can be understood that the maximum wall temperature difference for both particle distribution assumptions was not more than 1.4 K for all the heat fluxes considered. The reason can be:

- Simultaneous developing of both concentration and temperature profiles

Since the concentration profile is still developing along the length, the deviation of concentration from the average value (0.3) is not immediate. Figure 3-14 shows the concentration profile at a distance of 35 μm from the center (x/W = 0.7) along the length of the channel from inlet for PAO. It can be observed that the minimum value of particle concentration at the wall is 0.23, which happens to be at the exit. Figure 3-15 shows the resultant local wall temperature from inlet to exit, assuming both homogeneous and developing particle distributions. It can be observed that the local wall temperature for both cases is same up to a certain length of the channel. The difference in temperature profiles for both cases will be the combined effect of thermal boundary layer and particle distribution development, which is negligible for a certain length of the channel. It should also be noted that, once the local temperature is higher than the melting range, PCM latent heat is already used up and the effect of migration does not possibly affect the wall temperature. Hence, the difference in particle distribution for both assumptions might not have affected the thermal performance considerably.

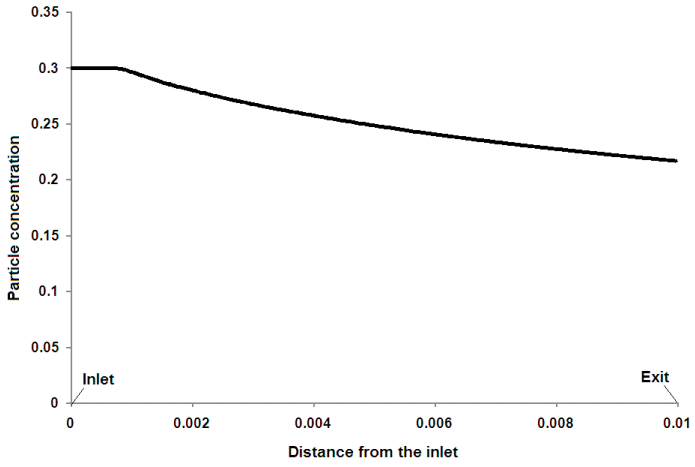

Figure 3-14. Particle concentration profile development along the channel

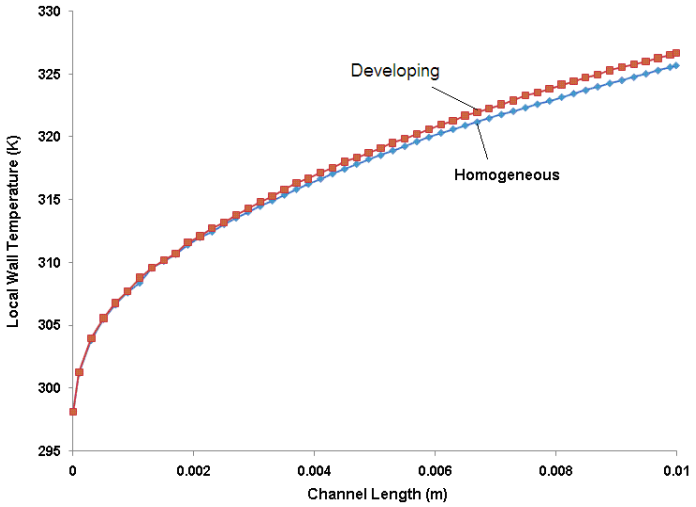

Figure 3-15. Local wall temperature for both profile assumptions along the channel

Another observation from the results is that the maximum wall temperature for developing profile assumption is lower compared to maximum wall temperature with homogeneous assumption in case of water. For PAO, this behavior was found to be opposite. The reason for this behavior can be the effective thermal conductivity of the fluid at the wall. In

case of water, when homogeneous assumption was used, the thermal conductivity was lower at the wall resulting in less heat transfer from wall to fluid and hence high wall temperature compared to developing profile assumption. This behavior is reverse for PAO, i.e., the thermal conductivity is higher when homogenous assumption was used and hence lower wall temperature compared to developing profile assumption.

From the above analysis, it can be observed that the maximum error in predicting the wall temperature is around 1.4 K for the conditions used, if a homogeneous assumption is used instead of nonhomogeneous assumption. This value was obtained for water at a heat flux of 20 W/cm^2, and the value of $T_{wall} - T_{in}$ is 29.2 K for developing profile and 30.6 K for homogeneous profile. In practical applications, this small temperature difference can be neglected owing to the many assumptions used in numerical simulations. Unless very accurate prediction is needed, including the particle migration effect is not very crucial.

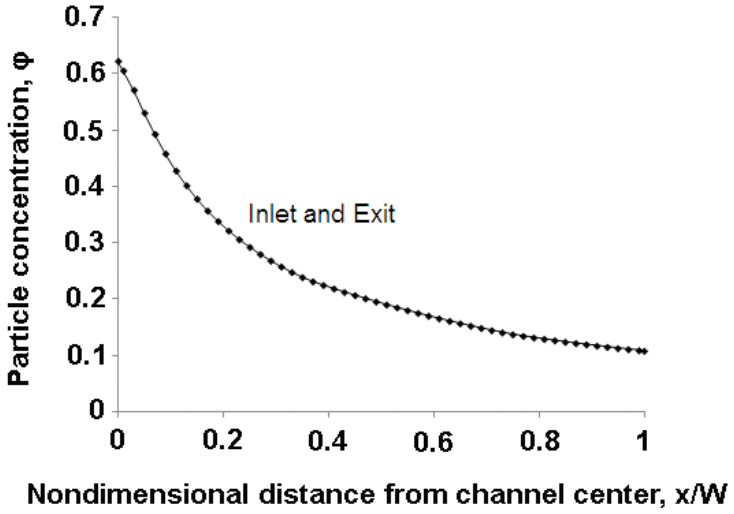

Figure 3-16. Particle concentration profile for fully developed assumption

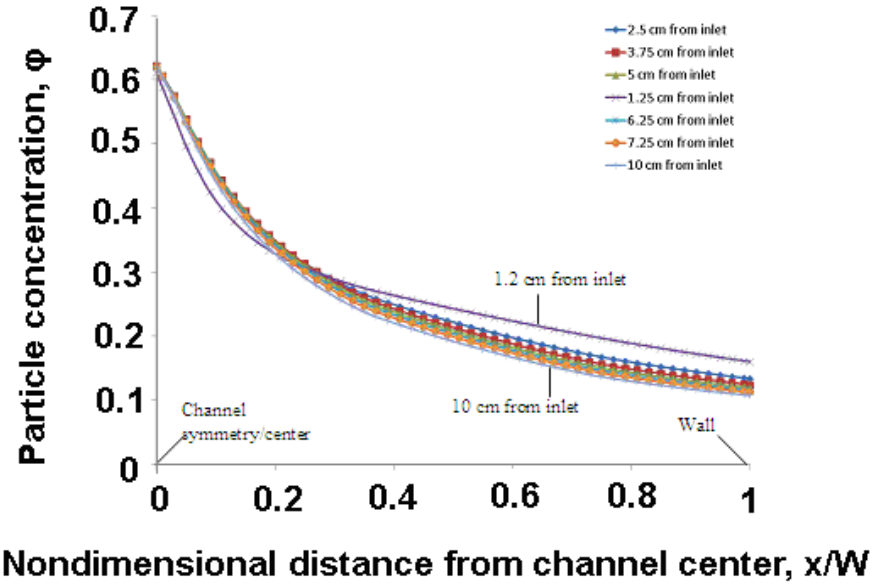

Figure 3-17. Particle concentration profiles at various lengths from inlet (base fluid - PAO)

3.5 Thermal Performance with Fully Developed Profile Assumption

Since a major difference was not observed in developing and homogeneous profiles, another set of simulations were run to compare the thermal performance of slurry when the particle distribution is assumed homogeneous and the particle distribution is fully developed (Figure 3-16). Particle diameter used is 5 µm, particle concentration is 0.3 and Re_{max} is 160. Fluid used is PAO. For parametric study the effect of inlet temperature, base heat flux, melting range were studied. Figure 3-17 shows the concentration profiles at different lengths from inlet. From the figure, it can be observed that the particle migration rate reduces significantly after certain length from the inlet. The particle concentration profile varied rapidly from inlet up to 2.5 cm length and the change in concentration profile variation from 2.5 cm to 10 cm is very slow. The difference between profiles at a length of 7.25 cm from inlet and 10 cm from inlet is negligible. Hence, it can be assumed that the particle profile is fully developed.

3.5.1 Effect of fluid inlet temperature

The inlet temperature of the fluid was first varied at a heat flux of 20 W/cm^2 and melting range of 5 K (25.5 ^{0}C to 30.5 ^{0}C, and peak is 27 ^{0}C). Figure 3-18 shows the results. It can be observed that an inlet temperature of 26 ^{0}C (slightly after lower melting point) will be useful in obtaining the maximum thermal performance at any profile assumption. The wall temperature difference between homogeneous and fully developed profile assumptions is around 3.6 K, where as the difference between homogeneous and developing profile assumptions is 1 K.

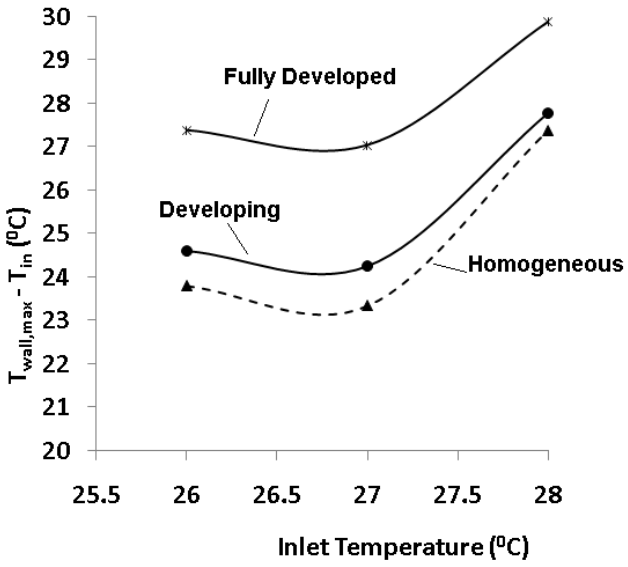

Figure 3-18. $T_{wall,\ max} - T_{in}$ vs. T_{in} for three assumptions at different inlet temperatures

3.5.2 Effect of wall heat flux

Figure 3-19 shows difference between maximum wall temperature and inlet temperature for all the three assumptions. It can be observed that the wall temperature difference is maximum

between fully developed and homogeneous assumptions at a heat flux of 30 W/cm^2. When the heat flux is increased to 40 W/cm^2 and 50 W/cm^2, the bulk temperature of fluid at the outlet is near the melting end temperature (making the PCM specific heat compared to PAO) and hence the effect of migration decreases.

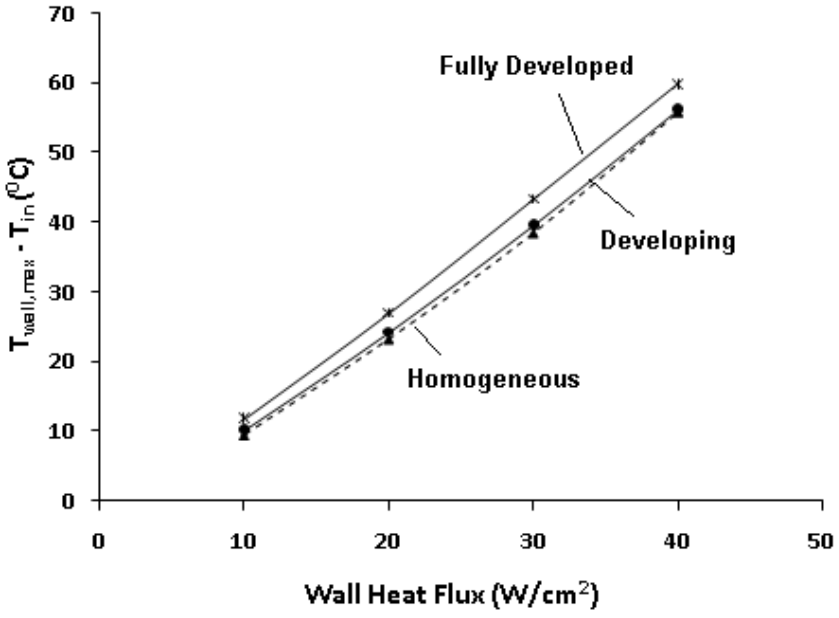

Figure 3-19. $T_{wall} - T_{in}$ for three profile assumptions at different heat fluxes

3.5.3 Effect of PCM melting range

Five different melting ranges were considered for the study. Figure 3-20 shows the result of varying melting range. It can be observed that thermal performance variation between homogeneous and nonhomogeneous assumptions decrease with increase in melting range. This can be due to lowered specific heat peak (because of averaging over a large melting range) which

makes the latent heat effect of PCM comparable to specific heat of base fluid. Therefore, the effect of migration of PCM particles to center diminishes with increase in melting range.

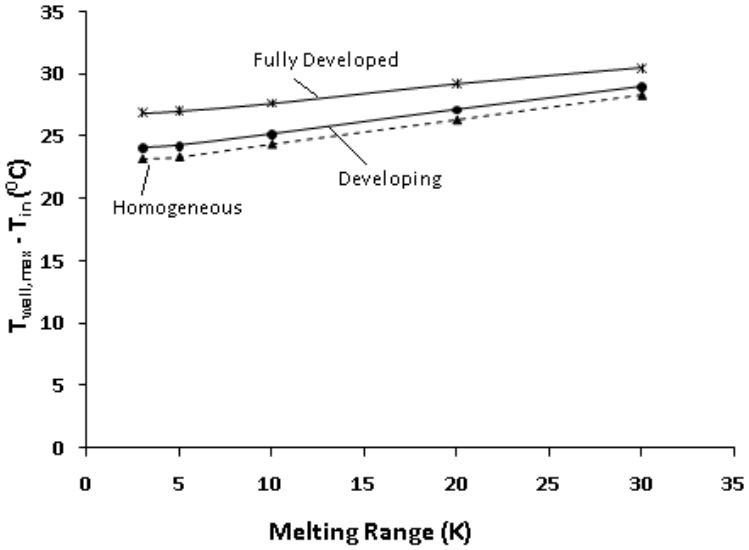

Figure 3-20. $T_{wall,\ max} - T_{in}$ for all three profiles at different melting ranges

Since a typical microchannel can also be 2 cm length, few more simulations were run to compare the thermal performance of slurry with developing profile and homogeneous profile. Figure 3-21 shows the comparison of wall temperature for both assumptions when the channel length is 2 cm. The maximum wall temperature difference between both profile assumptions was 1.2 K as compared to 1 K when the channel length was 1 cm.

The thermal performance of slurry was also analyzed in a 3D channel of 100 μm width, 1 mm height and 1 cm length. This was done to compare the maximum wall temperature obtained in 3D and 2D simulations. A base heat flux of 200 W/cm^2 (equal to 20 W/cm^2, at the wall for 2D) was used for 3D thermal simulations. Table 3-3 below shows the difference between 2D and 3D results for all the three assumptions. It was found that the maximum temperature of the wall

(fluid-solid boundary in width direction) is slightly lower than the wall temperature predicted using 2D. This is because in case of 3D, the increase in wall heat transfer area because of the addition of the base results in a lower wall temperature.

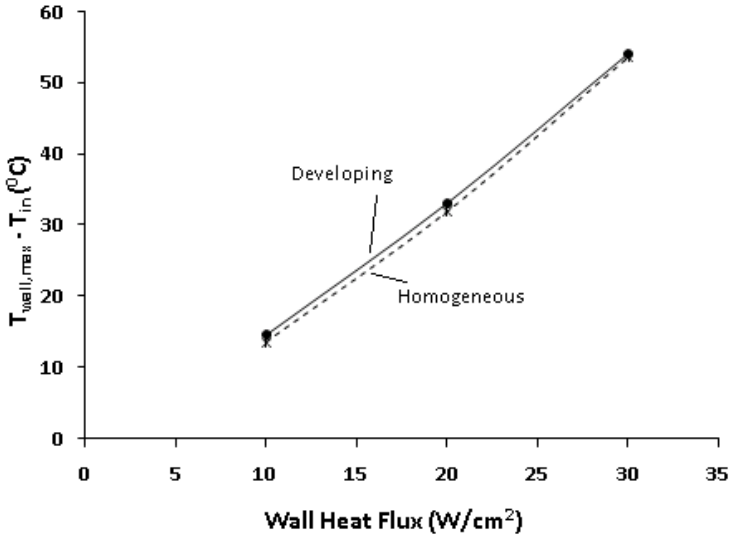

Figure 3-21. Results at a channel length of 2 cm

Table 3-3. Thermal results obtained in 3D using 2D particle distribution

Analysis	$T_{wall, HNT}$	$dT_{bulk, HNT}$	$T_{wall, NH}$	$dT_{bulk, NH}$	$T_{wall, H}$	$dT_{bulk, H}$
3D	322.34	300.94	324.56	301.04	322.03	300.87
2D	323.41	299.94	326.19	300.12	322.49	299.95

It should be noted that though in case of fully developed profile, the error in wall temperature prediction can be as high as 5 K for current simulations, in order to achieve the profile the length of the microchannel must be much larger compared to the typical 1 cm to 2 cm

length. Hence, it can be concluded that it is not important to include the particle migration in the numerical model.

CHAPTER 4 : PARAMETRIC STUDY – I

The parametric study is presented in two parts. First part includes the formulation of numerical model and some results that were obtained in microchannels assuming water and PAO as base fluids. This was done before the experiments were performed and hence the model was validated with experiments in prior literature. Second part includes the experimental study and parametric study done based on the experimental results.

4.1 Simulation Domain

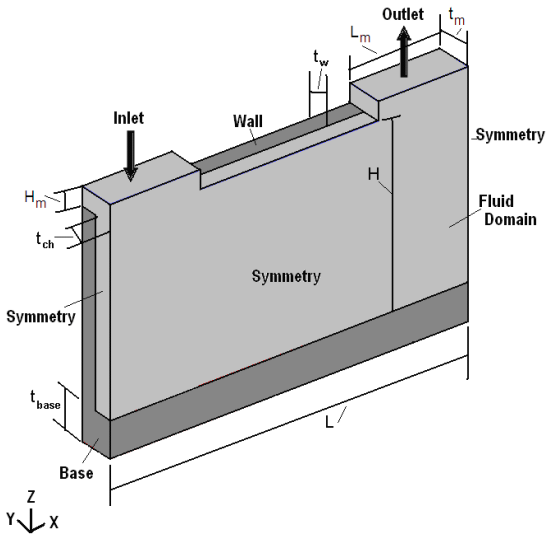

Figure 4-1. Schematic of flow domain

Figure 4-1 shows the schematic of the heat sink domain that was considered for parametric study. The flow rate at the entrance/inlet of the channel will be the total flow rate at the heat sink inlet divided by the total number of channels, assuming the same amount of flow

rate enters each channel. Only half of the channel was considered for simulation due to symmetry. The dimensions of the inlet and outlet manifolds are 200 μms in width (y-direction), 50 μm in height (z-direction) and 250 μm in length (x-direction). The microchannel dimensions are 100 μm in width (y-direction), 500 μm in height (z-direction) and 1000 μm in length (x-direction). The wall thickness was assumed to be equal to the microchannel width and the thickness of the base is chosen as 100 μm. It was assumed that there are 800 microchannels in each heat sink and the flow rate is assumed to be same at the inlet of each channel.

4.2 Assumptions

All the assumptions mentioned in Chapter 3 along with the following are used for formulating the problem.

i. The particle distribution is homogeneous. This is valid as explained in Chapter 3.

ii. Particle always follow the fluid

iii. The total volumetric flow at the inlet of heat sink is equally divided and is same in each channel.

4.2.1.1 Validation of assumptions major assumptions

- Assumption ii: Particles always follow the fluid

The amount of time taken by any particle to reach the fluid velocity can be calculated using Equation 4.1.

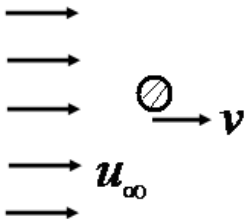

Figure 4-2: Drag on a spherical particle in a fluid field

Using the drag force on the particle (Figure 4-2) [60]:

$$F_D = m\frac{dv}{dt} = 6\pi\mu_f R_p(u_\infty - v) \tag{4.1}$$

Integrating the equation and using v = 0 at t = 0, to find the integration constant, Equation 4.1 becomes:

$$t = \frac{2}{9}\frac{\rho_p {R_p}^2}{\mu_f}\ln\left(\frac{u_\infty}{(u_\infty - v)}\right) \tag{4.2}$$

Defining the time constant as in Equation 4.3, the above equation becomes Equation 4.4:

$$\tau = \frac{2}{9}\frac{\rho_p {R_p}^2}{\mu_f} \tag{4.3}$$

$$\frac{u_\infty - v}{u_\infty} = e^{-t/\tau} \tag{4.4}$$

At $t = \tau$, $v = 0.63\ u_\infty$. This implies that the particle reaches 63 percent of fluid velocity in τ seconds. The time constant values for different particle diameters with water and PAO as base fluids is shown in Table 4-1. For the values below, the density of particle used is 774 kg/m^3, and dynamic viscosity of PAO and water used are 4.45×10^{-3} Pa.s and 7.39×10^{-4} Pa.s respectively.

Table 4-1. Time constant for different particle sizes

Particle diameter (μm)	τ_{water} (ns)	τ_{PAO} (ns)
0.1	0.57	0.09
1	57.50	9.64
5	1437.00	241.00

4.3 Governing Equations

With the assumptions mentioned above, the mass and momentum equations for slurry can be written as:

$$\frac{\partial u}{\partial x} + \frac{\partial v}{\partial y} + \frac{\partial w}{\partial z} = 0 \tag{4.5}$$

$$\rho\left(u\frac{\partial u}{\partial x}+v\frac{\partial u}{\partial y}+w\frac{\partial u}{\partial z}\right)=-\frac{\partial p}{\partial x}+\frac{\partial}{\partial x}\left(\mu\frac{\partial u}{\partial x}\right)+\frac{\partial}{\partial y}\left(\mu\frac{\partial u}{\partial y}\right)+\frac{\partial}{\partial z}\left(\mu\frac{\partial u}{\partial z}\right) \tag{4.6}$$

$$\rho\left(u\frac{\partial v}{\partial x}+v\frac{\partial v}{\partial y}+w\frac{\partial v}{\partial z}\right)=-\frac{\partial p}{\partial y}+\frac{\partial}{\partial x}\left(\mu\frac{\partial v}{\partial x}\right)+\frac{\partial}{\partial y}\left(\mu\frac{\partial v}{\partial y}\right)+\frac{\partial}{\partial z}\left(\mu\frac{\partial v}{\partial z}\right) \tag{4.7}$$

$$\rho\left(u\frac{\partial w}{\partial x}+v\frac{\partial w}{\partial y}+w\frac{\partial w}{\partial z}\right)=-\frac{\partial p}{\partial z}+\frac{\partial}{\partial x}\left(\mu\frac{\partial w}{\partial x}\right)+\frac{\partial}{\partial y}\left(\mu\frac{\partial w}{\partial y}\right)+\frac{\partial}{\partial z}\left(\mu\frac{\partial w}{\partial z}\right) \tag{4.8}$$

The energy equation for the slurry is:

$$\rho c_p\left(u\frac{\partial T}{\partial x}+v\frac{\partial T}{\partial y}+w\frac{\partial T}{\partial z}\right)=\frac{\partial}{\partial x}\left(k\frac{\partial T}{\partial x}\right)+\frac{\partial}{\partial y}\left(k\frac{\partial T}{\partial y}\right)+\frac{\partial}{\partial z}\left(k\frac{\partial T}{\partial z}\right) \tag{4.9}$$

Energy equation for the microchannel wall/fin is:

$$\frac{\partial^2 T_w}{\partial x^2}+\frac{\partial^2 T_w}{\partial y^2}+\frac{\partial^2 T_w}{\partial z^2}=0 \tag{4.10}$$

4.3.1 Boundary conditions

For flow inside the channels:

$$\mathbf{u} = 0 \text{ at the microchannel and manifold walls} \tag{4.11}$$

$$p = p_0, \text{ atmospheric pressure at the outlet} \tag{4.12}$$

$$\mathbf{u} = (0, 0, |w|) \text{ at the inlet} \tag{4.13}$$

For wall:

$$q.n = q_w; \text{ constant heat flux at the base of the fin} \tag{4.14}$$

$$q.n = 0; \text{ adiabatic on all other outer walls} \tag{4.15}$$

For fluid:

$$T = T_{in} \quad \text{at the inlet} \tag{4.16}$$

$q.n = (\rho c_p \mathbf{u} T).n$; convective heat flux boundary condition at the outlet/exit (4.17)

For wall and liquid interface:

$$T_w = T; \text{ continuity of temperature} \quad (4.18)$$

$$-k_w \frac{\partial T_w}{\partial n} = -k_f \frac{\partial T_f}{\partial n}; \text{ continuity of heat flux} \quad (4.19)$$

4.3.1.1 Dynamic viscosity

For suspensions that exhibit Newtonian characteristics, the bulk viscosity can be calculated from an empirical formula in terms of the particle concentration. Rutgers [61] has made an extensive survey and has suggested the following correlation by Vand [62, 63].

$$\frac{\mu_b}{\mu_f} = (1 - c - 1.16c^2)^{-2.5} \quad (4.20)$$

This correlation is derived for spherical particles and is valid for both small and large particle concentrations. In reality, the shape of the encapsulated particles might not be perfectly spherical and hence the viscosity can be different. It can be observed that from Table-1 of [26],

the measured experimental viscosity values deviate from the values obtained using Vand's correlation. This difference increases with increase in particle concentration.

4.3.2 Validation of numerical model

The current numerical analysis mainly models the slurry with bulk properties using the effective specific heat method mentioned in [31]. Since there are no experiments performed inside the MMC channels using PCM slurries, the results could not be validated directly. However the effective specific heat method was first used to simulate the experiments performed in [16] where the slurry is passed through a tube with inner diameter of 3.14 mm and the length of the tube is 0.3 m. The flow is heated with a constant heat flux source. Figure 4-3 shows the comparison of the current model (effective specific heat method) with that of the experimental results of [16].

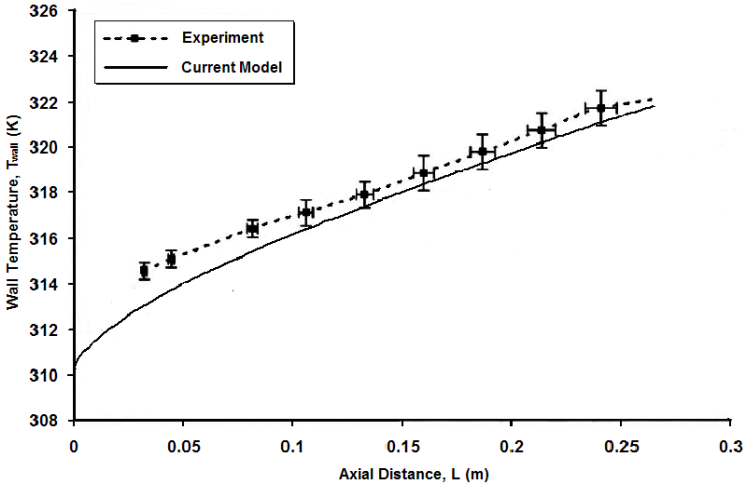

Figure 4-3. Comparison of results using current model with experiments in [13];

$c = 0.1$, Ste = 3.0, Re = 200, $d_p = 100$ µm

A two dimensional axisymmetric computational domain was used for solving the temperature along the tube. A constant inlet temperature boundary condition was used. The other boundary conditions that were used are axial symmetry along the axis, constant heat flux along the tube radius or wall and a convective heat flux boundary condition at the outlet. A fully developed parabolic profile was assumed at the inlet. Parameters used for the simulation are 100 μm particle diameter, 0.1 particle concentration, a Reynolds number of 200 and a Stefan number of 3.0. The thermophysical properties used are shown in Table 4-2.

Table 4-2. Thermophysical properties used for simulation of experiments in [16]

Property	Water	Eicosane
Density (kg/m^3)	997.07	778 (liquid) 856 (solid)
Viscosity (Pa.s)	8.904x10^{-4}	–
Specific heat (J/kg.K)	4179.6	2250 (liquid) 1773 (solid)
Thermal conductivity (W/m.K)	0.606	0.15 (liquid) 0.2583 (solid)
Latent Heat (J/kg)	-	247 x10^3

Different melting ranges of 1.8 K, 2 K, 2.4 K and 3 K were used for the simulation. There was a slight difference in the results for all the melting ranges used. The figure shows the plot of temperature when the melting range was 1.8 K, with inlet temperature equal to 308.95 K. In [16], the melting range and the inlet temperature of the slurry were not specified. The inlet temperature for all these simulations was taken at the start of melting (equal to T_1). This was

done to ensure that all the latent heat of the phase change material was used. It can be observed that the current numerical model predicts the behavior well.

4.4 Results: Parametric Study – I

For all the simulations, in the dissertation work, the grid independency check was performed. The tolerance values used were 1e-5 for both velocity and temperature. Two different slurries with base fluids, water and PAO and n-Octadecane as the phase change material (melting point 27 ^{0}C) were used for simulation. The properties of PAO used for simulation are shown in Table 4-3 and are evaluated based on the equations in [64]. The wall material used for simulation is copper. The properties of Octadecane used are that of solid PCM.

Table 4-3. Thermophysical properties of suspension components used for parametric study – I

Property	Copper	Water	PAO	Octadecane
Density (kg/m^3)	8700	994	784	774
Viscosity (Pa.s)	-	7.39×10^{-4}	4.45×10^{-3}	–
Specific heat (J/kg.K)	385	4180	2242	2180
Thermal conductivity (W/m.K)	400	0.62	143×10^{-3}	0.15
Latent Heat (J/kg)	-	-	-	244×10^{3}

The pressure drop values obtained were found to match with theoretical predictions presented in [65]. The bulk mean temperature rise values were checked with heat balance

between the source and fluid sensible heat for all the cases with pure PAO. The difference between the calculated bulk temperature rise and the obtained temperature rise using numerical simulation is less than 0.1 K. Two different bulk temperature rise values were calculated in case of slurry as the exact amount of latent heat utilized and hence the specific heat is unknown for doing the energy balance between the source and the sink. One value of specific heat was calculated assuming the latent heat is being used (particle temperature is equal to T_m) and the other using pure solid/liquid specific heat. It was found that the temperature rise obtained using the numerical simulation lies between the two bulk temperature rise values calculated using energy balance. Thus, it was assumed that the global energy balance is satisfied. The bulk mean temperature of the fluid at the exit is calculated (density is a constant) as:

$$T_{exit} = \frac{\int T * c_{p,eff} * (n.\vec{u}) ds}{\int c_{p,eff} * (n.\vec{u}) ds} \tag{4.21}$$

where, *ds* is the surface area at the outlet.

Unstructured grid generated using the free mesh option in COMSOL was used for solving the velocity and temperature fields. Mesh consisted of tetrahedral elements and the number of elements was 17270. The results were checked for grid independency with a refined mesh consisting of 61641 elements. The maximum temperature difference in the results with refined mesh was around 0.15 K and there was no difference in velocity gradients. The mesh was further refined (with 203954 elements) and the temperature difference was found to be negligible compared to the results obtained with mesh consisting of 61641 elements.

For all the cases with mass concentration greater than zero, the enhancement in thermal conductivity due to the presence of NEPCM particles was calculated. The flow field was first solved and the velocity gradients were exported to Matlab® [66] to calculate the effective thermal conductivity. This data was then used to solve the temperature field. The enhancement in the thermal conductivity was found to be negligible for the current simulation cases since the particle diameter is small. However, for large particle diameters, this enhancement in thermal conductivity is large and it is important to consider while solving the problem [31]. Figures 4-4 and 4-5 show the plots of velocity and temperature profiles inside MMC channel. It can be observed that the flow inside the channel is not hydrodynamically and thermally developed.

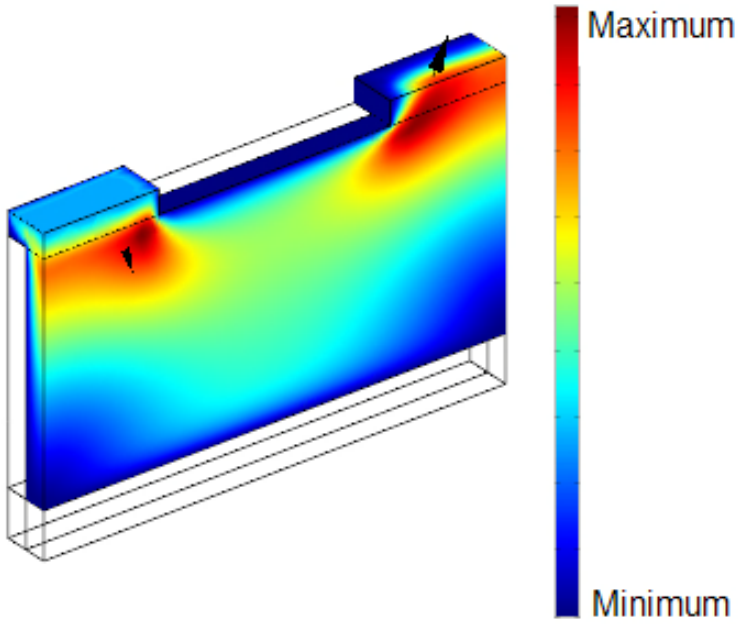

Figure 4-4. Velocity profile inside the flow domain

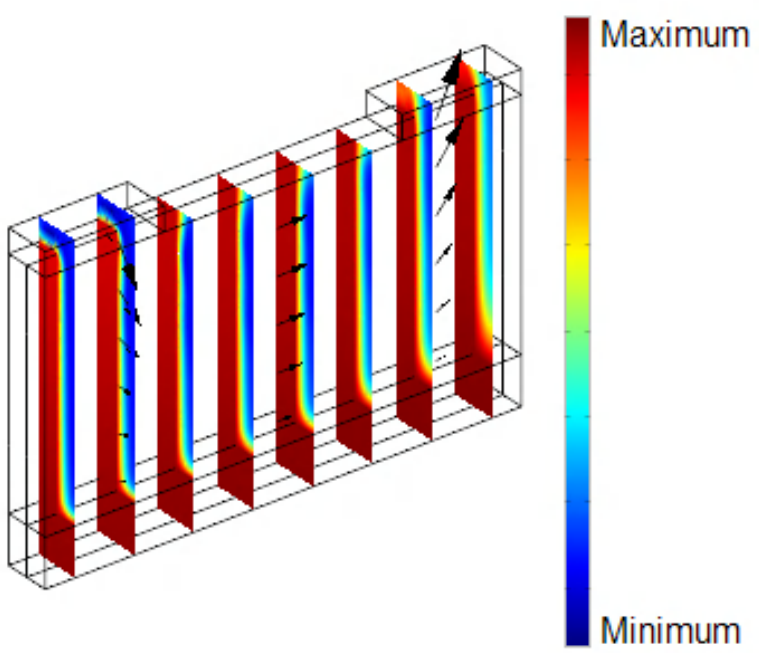

Figure 4-5. Temperature profile inside the flow domain

4.4.1 Results with water as base fluid

For simulations with water as base fluid in parametric study – I, the mass flow rate at the inlet of heat sink was assumed to be 0.017 kg/s. Particle mass concentration was varied from 0 to 0.3 and a heat flux of 500 W/cm^2 was used at the base of the channel. A melting range of 10 K and inlet temperature of 22.2 ^{0}C was used for simulation. Figure 4-6 shows the resultant pressure drop with increase in particle mass concentration. The pressure drop increases with particle concentration due to increase in viscosity.

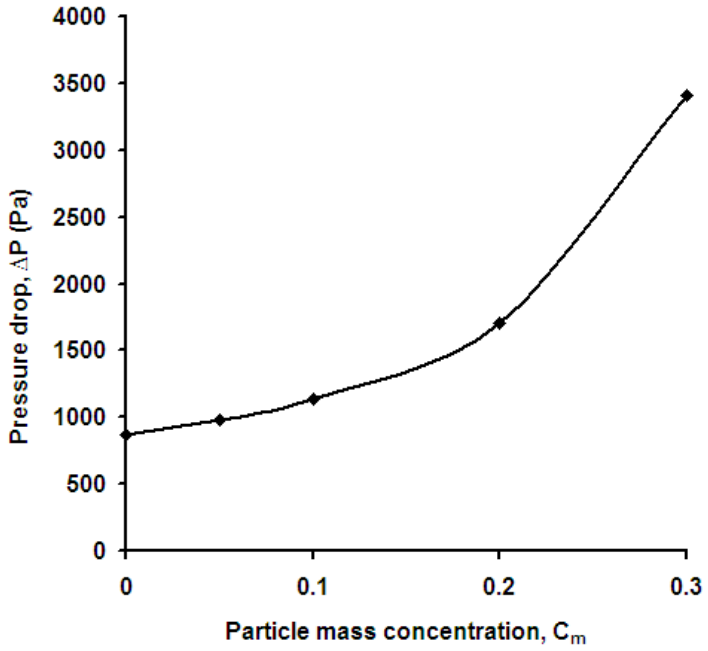

Figure 4-6. Pressure drop inside the channel as function of particle concentration

Bulk temperature rise of slurry decreases with increase in particle mass concentration (as shown in Figure 4-7) due to the increase in effective specific heat capacity of the fluid during melting. Figure 4-8 shows the heat transfer coefficient ratio defined as in Equation 4.22 with increase in concentration.

$$h_r = h_{slurry}/h_{\text{ base fluid}} \tag{4.22}$$

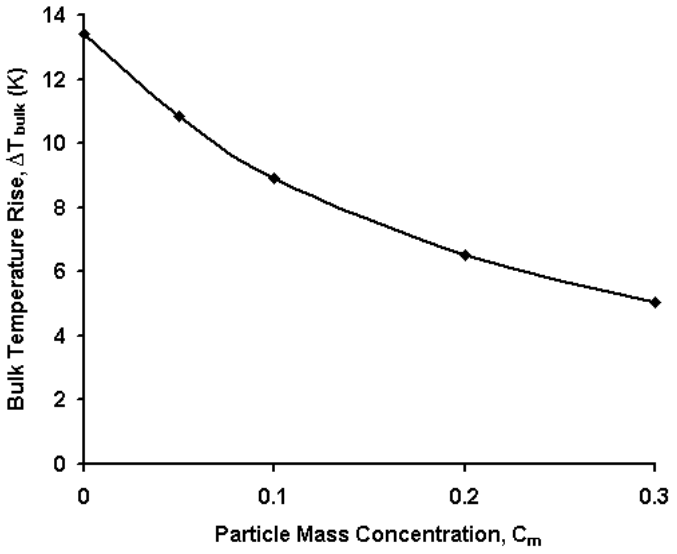

Figure 4-7. Bulk temperature rise as function of particle concentration

From the figure, it can be observed that the heat transfer coefficient of slurry decreases with increase in particle concentration. The poor performance of slurry compared to water at all the flow rates can be due to:

- Low thermal conductivity of slurry compared to water

Presence of PCM particles increase the heat capacity of the fluid (during melting), but also decrease the effective thermal conductivity and sensible heat capacity. In case of fully developed flows, high specific heat fluid always performed better as shown by many researchers. This is because, the heat has already reached the center of the channel and the effect of high specific capacity of the fluid dominates the effect of lowering of thermal conductivity due to presence of PCM. When the flow is not thermally fully developed, the heat transfer performance of slurry depends how effectively the heat is transferred to the fluid. Low thermal conductivity results in less heat transfer to the fluid.

Since water based slurry did not perform better compared to pure water, next set of simulations were done with PAO as base fluid. Further parametric study was done by varying the inlet temperature, PCM concentration, heat flux and melting range of PCM.

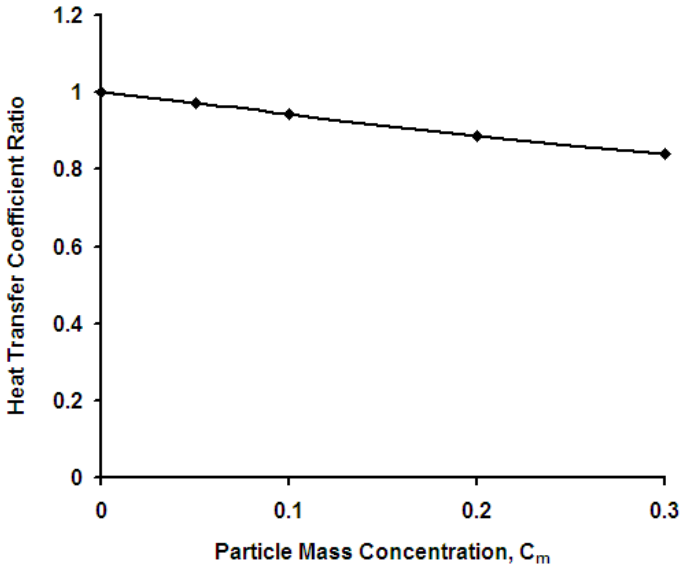

Figure 4-8. Heat transfer coefficient ratio

4.4.2 Results with PAO as base fluid

Since the properties of PAO are function of temperature, the pure case of PAO was first run using varying properties and then with average properties for a mass flow rate of 20.8×10^{-6} kg/s and a heat flux of 100 W/cm^2. Table 4-4 shows the results with varying properties and constant average properties. As can be seen from the table, the difference between the heat transfer results for both cases is about 1%. The difference in the pressure drop results is less than 5%. Hence average properties of PAO were used for the simulation. The mass flow rate of the fluid used at the inlet is 10.4×10^{-6} kg/s, for all the parametric study cases with PAO as base fluid.

Table 4-4. Comparison of results for pure PAO with varying properties and average properties

PAO properties	ΔT_{bulk} (K)	Nu_m	ΔP (Pa)
Varying Properties	4.10	51.0	5585
Constant Properties (evaluated at 28.8 ^{0}C)	4.14	50.5	5861

4.4.2.1 Effect of particle mass concentration

For investigating the effect of particle mass concentration, the melting range of PCM used is 10 K. The heat flux used is 100 W/cm^2. The pressure drop from the inlet to the outlet with change in PCM concentration is shown in Figure 4-9. The pressure drop from the inlet to outlet increases with increase in concentration. The simulations show that the bulk mean temperature rise of slurry is always lower than the pure fluid. The higher the concentration of PCM in slurry, the lower is the temperature rise. Figure 4-6 shows the bulk mean temperature rise from inlet to the exit as a function of PCM concentration considered when the inlet temperature of the fluid is equal to T_m. The summary of results for cases considered is shown in Table 4-5. From the table it can be observed that if the bulk mean temperature rise for pure PAO is desired to be 0.65 K (which is the rise for slurry with c_m = 0.3), the mass flow rate must be increased around 12.7 times and the resulting pressure drop increases by 28.5 times. The heat transfer coefficient is found to increase with increase in concentration.

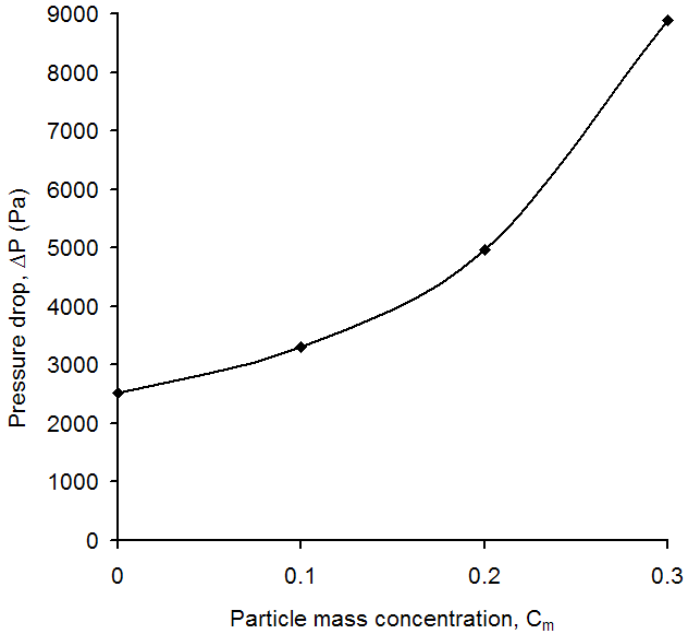

Figure 4-9. Pressure drop inside the channel as a function of particle mass concentration

Table 4-5. Effect of mass concentration

Fluid (c_m)	$\dot{m}$ **(x10^6)(kg/s)**	**ΔP (Pa)**	**ΔT_{bulk} (K)**
PAO (0)	10.4	2517	8.28
Slurry(0.1)	10.4	3310	2.64
Slurry (0.2)	10.4	4964	1.13
Slurry(0.3)	10.4	8894	0.63
PAO (0)	132.0	71706	0.63

($q = 100 W/cm^2$, $T_{in} = T_m$, $T_{Mr} = 10$ K)

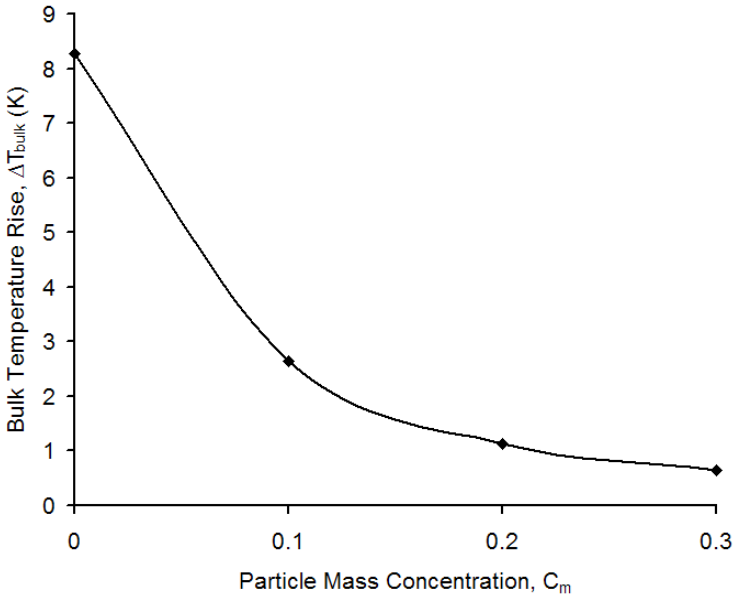

Figure 4-10. Bulk mean temperature rise as a function of particle mass concentration

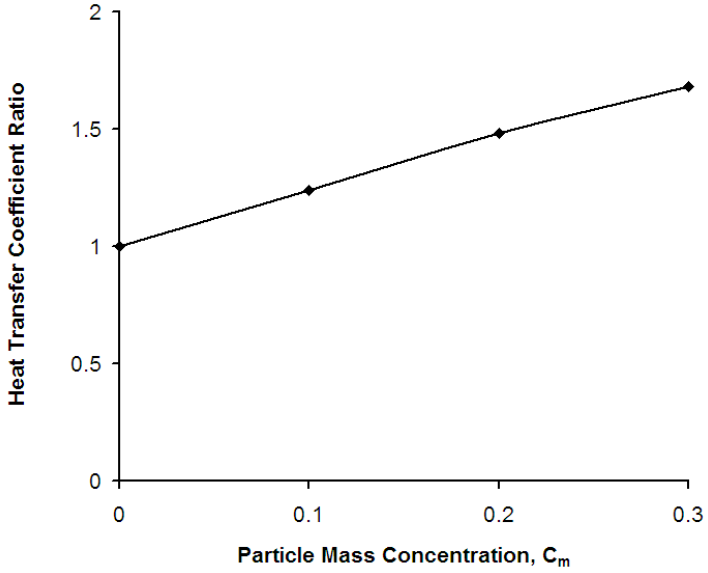

Figure 4-11. Heat transfer coefficient ratio as a function of particle mass concentration

4.4.2.2 Effect of inlet temperature and melting range

Since the PCM is assumed to have a melting range, it is interesting to observe the best case where the heat transfer enhancement is maximum and bulk mean temperature rise is minimum. Thus for a concentration of 0.3, at a heat flux of 100 W/cm^2, the inlet temperature was varied in order to find the best case. Figure 4-12 shows the bulk mean temperature rise of the fluid and Figure 4-13 shows the heat transfer coefficient ratio as a function of nondimensional inlet temperature for different melting ranges.

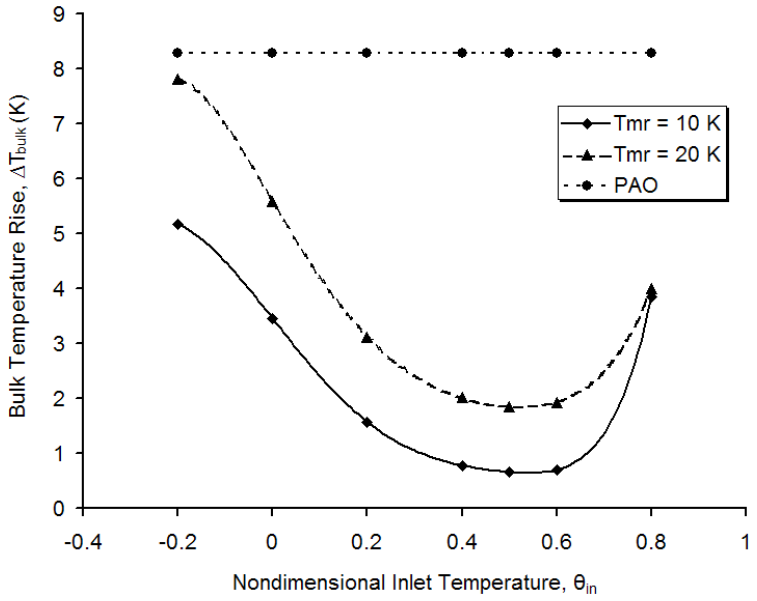

Figure 4-12. Bulk temperature rise with varying inlet temperature and melting range of PCM

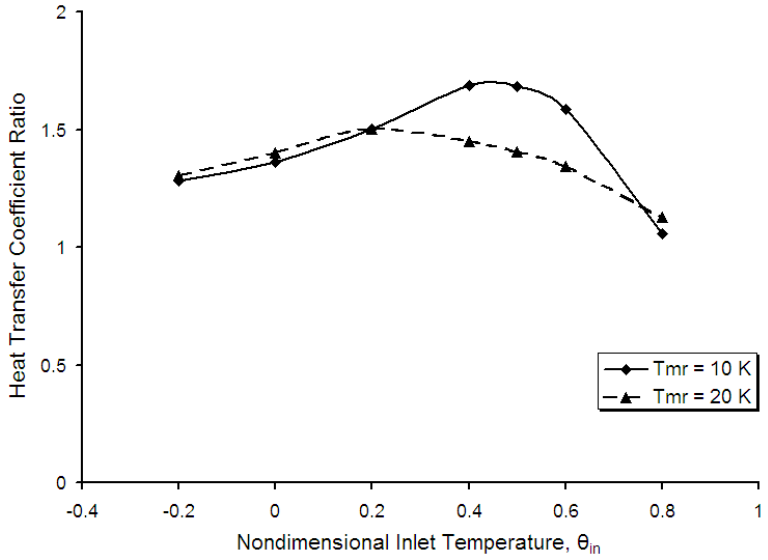

Figure 4-13. Heat transfer coefficient ratio with varying inlet temperature and melting range of PCM

The results presented were run for varying melting ranges. As can be seen from the figures, if the nondimensional inlet temperature of the fluid is 0.5 (T_{in} = T_m), the bulk mean temperature rise of slurry is better for both cases of melting range considered. But if the heat transfer coefficient ratio is considered, it depends on the melting range. In addition, if the melting ranges are observed, the narrower is the melting range, the better is the heat transfer enhancement. As the melting range depends on the purity of PCM, it can be concluded that the purity of PCM helps in increasing the heat absorbing capacity of the bulk fluid and the heat transfer.

4.4.2.3 Effect of base heat flux

The simulations were run for pure PAO and 0.3 concentration slurry for different heat fluxes at a nondimensional inlet temperature of 0.5. It can be observed that for high heat fluxes, the performance of slurry improves compared with pure PAO. The difference in the bulk temperature rise (Figure 4-14) between pure PAO and slurry increases with increase in heat flux whereas the heat transfer coefficient ratio (Figure 4-15) is always high for slurry for any case. It should also be noted that the hear transfer coefficient ratio depends on the heat flux. At a heat flux of 100 W/cm^2, the ratio is high compared to the other heat fluxes considered. The reason is the amount of PCM that is used for heat absorption dictates the heat transfer coefficient ratio.

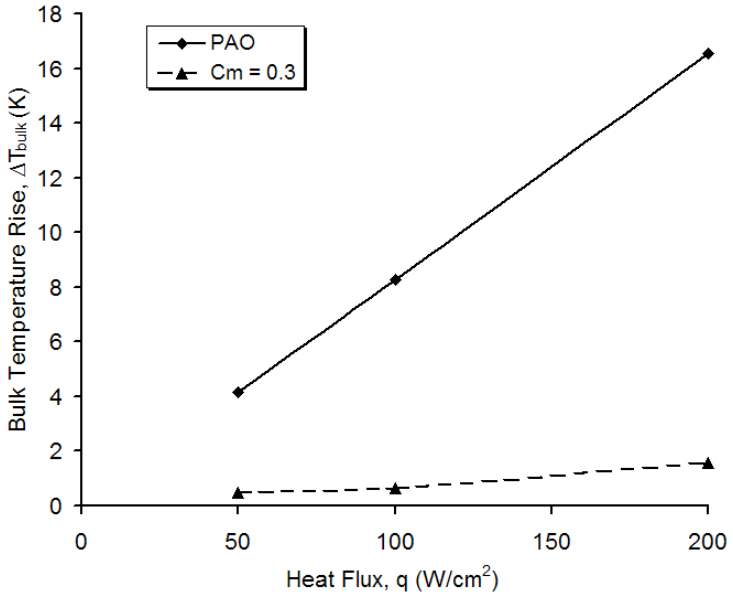

Figure 4-14. Bulk temperature rise for pure PAO and slurry at varying heat fluxes

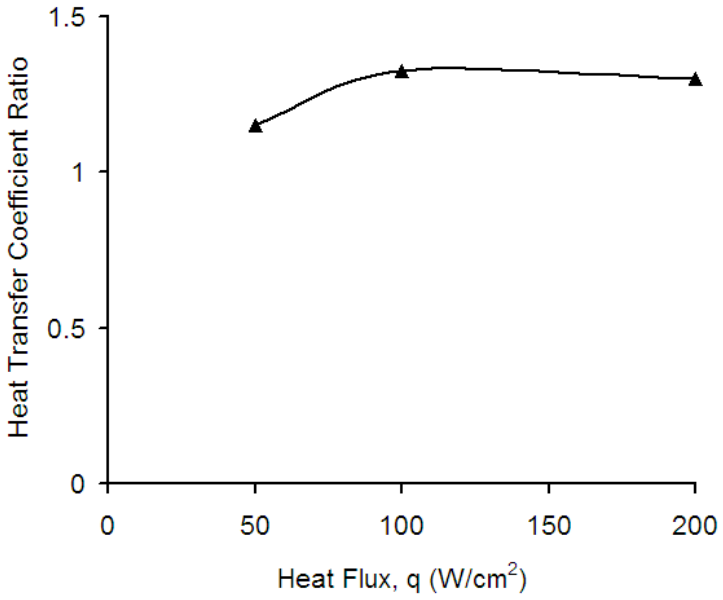

Figure 4-15. Heat transfer coefficient ratio for slurry at varying heat fluxes

Further numerical study will be presented in next Chapter after presenting the experimental results. The fabricated parts in case of experiments did not exactly have a channel width of 101 μm and height of 533 μm and hence the simulation domain is slightly different.

CHAPTER 5 : PARAMETRIC STUDY – II

From Chapter 3, it is evident that the particle migration effect is negligible and using NEPCM would help in instantaneous melting of the particle. Such small particles are not yet commercially available, and hence experiments were performed with slurry with an average particle diameter around 5 μm.

5.1 Experimental Study

Experiments were performed in custom fabricated microchannel heat sinks. These heat sinks were fabricated at Microcooling Concepts Inc. with an average foot print of 1 cm x 2 cm and are similar to the conventional manifold microchannel heat sinks. For illustration purposes, Figure 5-1 shows the possible fluid path and Figure 5-2 shows the photograph of the fabricated part. There are approximately 441 microchannels inside the heat sink and each channel is approximately is 101 μm wide, 533 μm high and 1 mm long.

MEPCM slurry made at BASF® was used and consisted of particles of size ranging from 1 to 5 μm with an average diameter of 4.97 μm mixed in water. The core material is n-Octadecane and the shell material is polymethylmetacrylate (PMMA). In [23], similar particles were used and it was mentioned that the measured viscosity values deviates from Vand's correlation [58, 59] that is usually used for calculating bulk viscosity. This equation is derived for spherical particles. In reality, as the particles are not spherical in nature, viscosity value predicted by this correlation may not be accurate. Hence the measured value provided in [23] was used (Table 5-1) for theoretical calculations and numerical simulation when simulating

experiment results. The latent melting enthalpy of PCM was measured using differential scanning calorimetry (DSC) and was found to be 120 kJ/kg between 23 ^{0}C and 29 ^{0}C. Figure 5-3 shows the DSC curve of the dried MEPCM particles. A heating rate of 5^{0}C /min was applied during the test. The sample size was 7 mg. The onset temperature is 23 ^{0}C and endset temperature is around 29 ^{0}C during the melting of the MEPCM. The peak melting temperature is around 27 ^{0}C. The latent melting enthalpy of the particles is 120 kJ/kg between 24 ^{0}C and 29 ^{0}C. It can be observed that the latent heat of these MEPCM capsules is considerably smaller than the core material. The reason might be the presence of capsules' shell material.

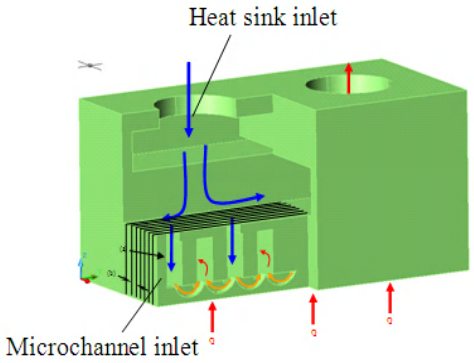

Figure 5-1. Possible fluid path in the fabricated microchannels

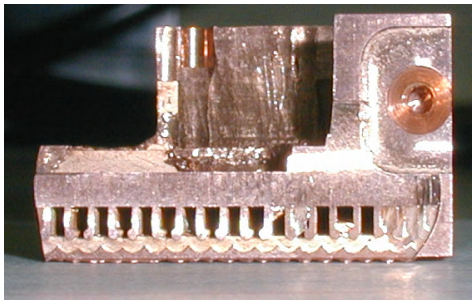

Figure 5-2. Cross-section of the fabricated heat sink

Table 5-1. Properties of the suspension components used for experiments

Component	Density, kg/m^3	Specific heat, J/kg.K	Thermal conductivity, W/m.K	Viscosity, kg/m.s	Latent heat kJ/kg
Water	997	4180	0.604	$1x10^{-3}$	-
MEPCM Particle	867.2	1899	0.164	-	120
Slurry (10%)	982.3	3951	0.541	$2.3x10^{-3}$	-

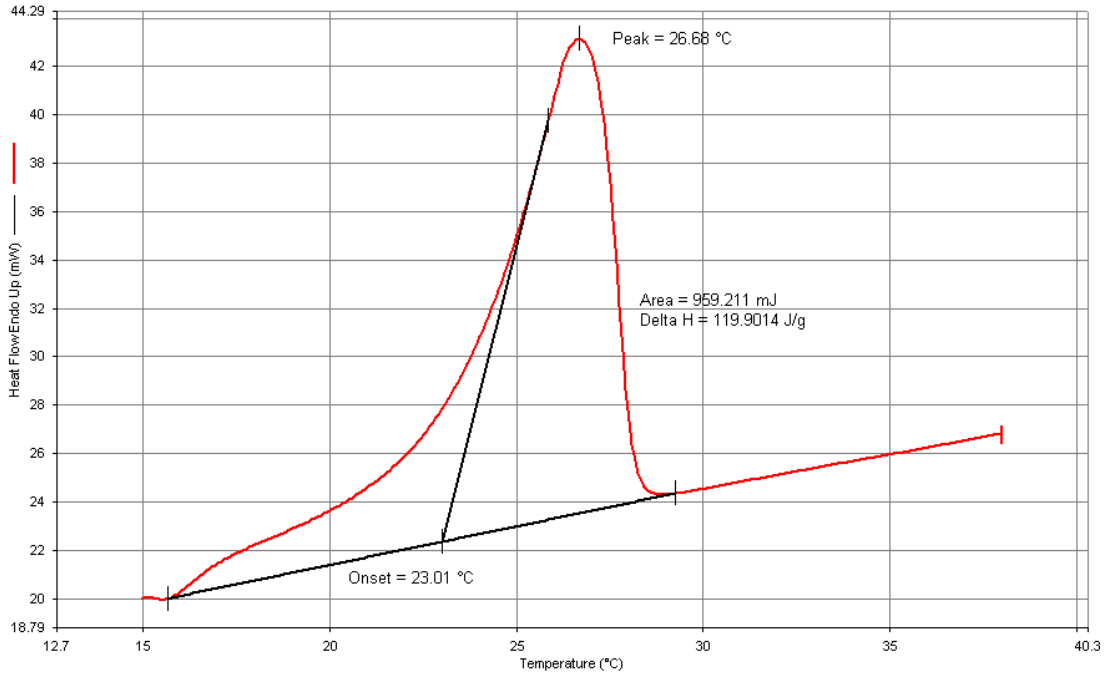

Figure 5-3. DSC of dried MEPCM particles used for thermal experiments

5.1.1 Test setup

Figure 5-4 illustrates the schematic of the flow loop for the experiments. It consists of microchannel heat exchanger, a pump, a valve, a flowmeter and two mixing sections at both inlet and outlet of the heat exchanger, a plate heat exchanger. Working fluid was pumped from the fluid reservoir using a diaphragm pump. The valve was used for flow rate adjustment in the loop.

The flow rate was measured using two Coriolis flow meters with scale of 20 GPH and 40 GPH (one is for small flow rate and one for large flow rate). The two mixing sections were used to mix fluid thoroughly so that the thermocouples measure the bulk temperature at the inlet and outlet of the heat exchanger.

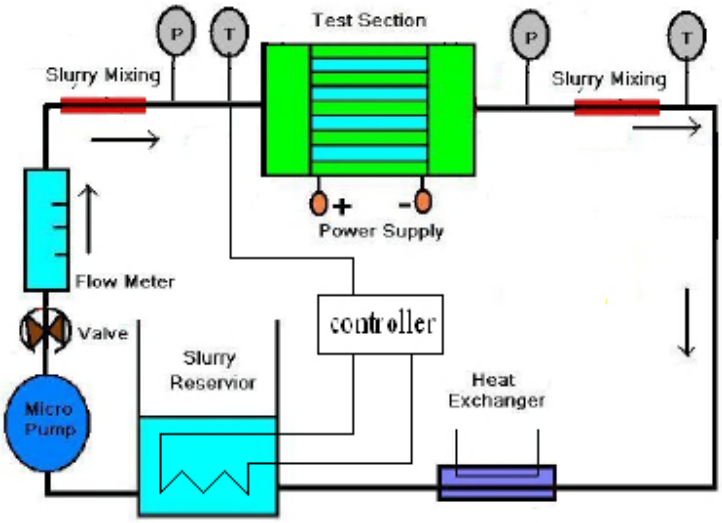

Figure 5-4. Schematic of the experimental setup

The plate heat exchanger was used to cool down working fluid after it leaves the test section. The temperature was set to below re-solidifying temperature of the PCM material. The heater in the reservoir was used to adjust the fluid temperature at the inlet of the microchannel heat exchanger. Two thin film resistors soldered at the bottom of the microchannel heat exchanger were used as heating source in the experiments. Power to the resistors was supplied by an adjustable DC power supply to vary the amount of heat generated by the heater. Two thermocouples were attached to the back of the thin-film resistors to measure the heater

temperature. Power to the heater was calculated by measuring the voltage across the heater and the current that passes through the heater. The resistors were thermally insulated in the experiments. Since most of the heat that is generated by the heater will be absorbed by the microchannel heat exchanger, it was assumed that the measured temperature at the heater is equal to the wall temperature of the heat exchanger. The temperature at the outlet of the plate exchanger was monitored so that working fluid is cooled below the re-solidifying temperature during the tests on slurry.

5.2.1 Experiment Results

Experiments were performed with pure water and slurry with particle concentration 0.1 (to avoid clogging). Figure 5-5 shows the pressure drop obtained across the heat sink at different inlet flow rates. Pressure drop of slurry is higher compared to water for all the flow rates due to the increase in viscosity of the fluid. Tables 5-2 and 5-3 show the experiment conditions and heat transfer results obtained with water and slurry.

Table 5-2. Heat transfer results (with water)

V_{HS} (GPH)	Q (W)	T_{in} (^{0}C)	T_{out} (^{0}C)	T_w (^{0}C)
10	360.1	33.8	42.0	70.3
12	360.4	35.2	42.3	70.3
15	360.5	34.2	40.0	67.2
17	360.1	34.4	39.4	66.3
20	360.6	33.1	37.1	63.3
24	360.3	37.0	40.2	65.7
27	360.3	35.6	38.5	63.8
30	360.7	33.2	35.9	60.6

Table 5-3. Heat transfer results (with slurry)

V_{HS} (GPH)	Q (W)	T_{in} (^{0}C)	T_{out} (^{0}C)	T_w (^{0}C)
5	183.6	22.1	32.8	53.9
8	183.6	24.6	31.5	51.4
10	360.1	23.6	32.6	67.5
12.5	360.4	24.9	32.0	64.7
15	360.5	25.2	30.7	61.6
17.5	360.1	24.9	29.4	59.5
20	360.6	24.8	28.6	58.2

Figure 5-6 shows the heat transfer coefficient of water and slurry at different flow rates. The heat transfer performance was evaluated by comparing the heat transfer coefficient defined as

$$h = \frac{Q}{A_b(T_w - T_{in})} \tag{5.1}$$

T_w is the wall temperature at the heater. It can be seen that heat transfer coefficient of slurry is lower than heat transfer coefficient of water (base fluid). The error in power calculation from the voltage and current measurement can be ignored in the experiments. The error in flow rate measurements was estimated to be less than 5%. The error in temperature measurement is within 0.2 ^{0}C. Thermal balance between supplied power to the heater and amount absorbed by working fluid in the water experiments was less than 6.3%. The error in heat transfer coefficient calculated based on the measurement was estimated to be less than 8%.

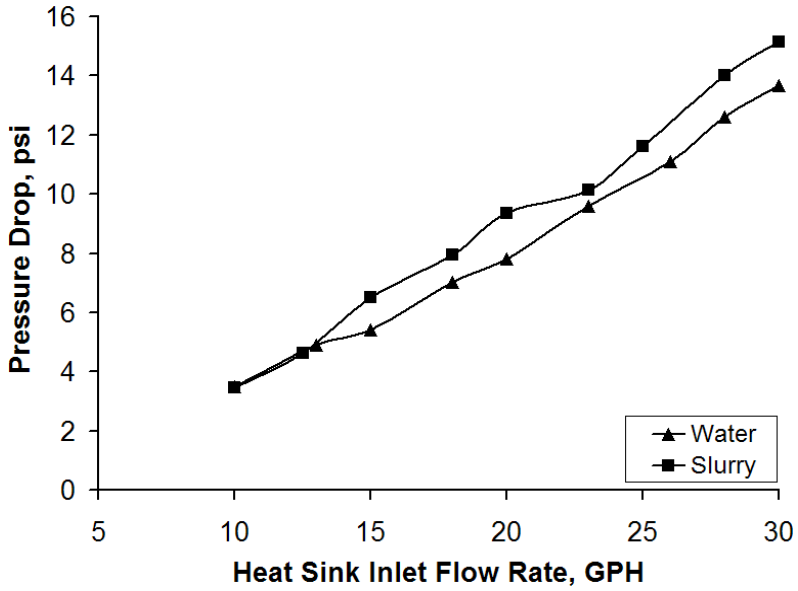

Figure 5-5. Experiment results – pressure drop

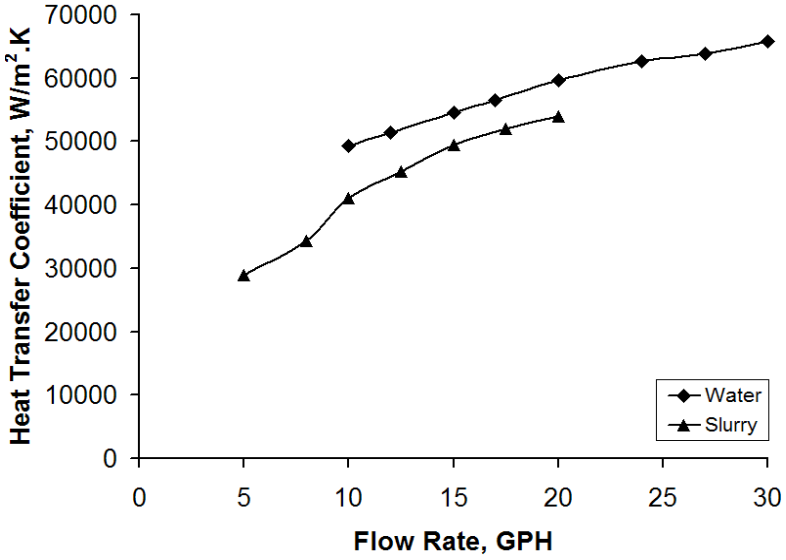

Figure 5-6. Heat transfer coefficient of water and slurry

5.2.2 Analysis of experiment results

The performance of slurry is poorer compared to pure water at all the flow rates. The possible reasons for this behavior of slurry could be due to:

- Low thermal conductivity of slurry compared to water

As discussed in Chapter 4, the resultant thermal conductivity of slurry is lower compared to pure water and hence the heat transfer from wall to the fluid in case of slurry is lower.

- Little or no melting of PCM particles inside the channel

Since the length of the channel is short for the MMC channel, it is important that the PCM particle completely melts within its residence time. Figure 5-7 shows the required temperature difference between the fluid and the particle melting temperature for a 5 μm diameter particle at different velocities. A velocity of 0.25 m/s corresponds to V_{HS} = 5 GPH, lowest flow rate used in the experiments. Since the flow is not fully developed thermally, it is highly possible that a large portion of the fluid remained at the inlet temperature and this required temperature difference could not be achieved for all the particles inside the channel.

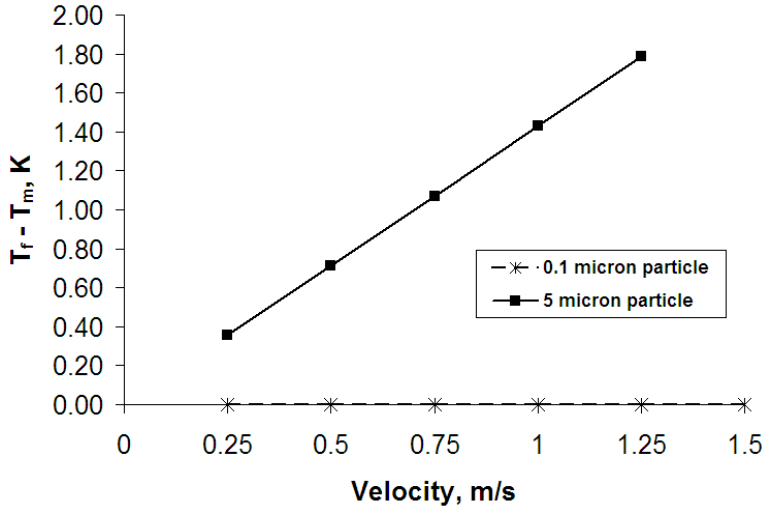

Figure 5-7. Required temperature difference between particle surface and PCM melting temperature

5.2 Numerical Results

Configuration I of Table 5-4 is used for numerical simulation while comparing with experiment results. Since the average particle diameter is 4.97 μm, the same value was used. Copper is used as the wall material.

Table 5-4. Geometric configurations used for numerical simulation (units in μm)

Configuration	Base fluid	H	$2*t_{ch}$	L	H_m	$2*t_m$	L_m	$2*t_w$	t_{base}
I	Water, PAO	533	101	1000	50	201	250	352.52	250
II	Water, PAO	375	25	1000	100	100	250	75	250

The flow rate at the microchannel inlet was calculated based on the number of channels and total flow rate at the inlet of the heat sink. The wall thickness of the microchannel was used such that the base heat flux and the total heat supplied is the same as in experiments. In other words, twice the base area in the simulation domain multiplied by number of channels is equal to

the base are of the heat sink, which is 2 cm^2. Pressure drop and bulk temperature rise obtained in both cases are presented in Table 5-5. Pressure drop predicted numerically ranges from 8.3 to 13.0% of total pressure drop obtained in experiments. This suggests that the pressure drop inside manifolds is higher compared to that of pressure drop inside the microchannels, which could be due to poor manifold design. Proper design of the heat sink can result in more than 90% of pressure drop inside microchannels and less than 10% in manifolds.

Table 5-5. Numerical results obtained

Fluid	V_{HS} (GPH)	Q (W)	T_{in}(°C)	ΔT_{bulk}(°C)	ΔP (psi)
Water	5	183.6	22.1	8.5	0.10
Water	10	360.1	33.8	8.3	0.29
Water	15	360.5	34.2	5.8	0.62
Slurry	5	183.6	22.1	8.9	0.18
Slurry	10	360.1	23.6	8.7	0.45
Slurry	15	360.5	25.2	6.1	0.81

Figure 5-8 shows the heat transfer coefficient obtained with numerical simulation and comparison with experiment results. The predicted maximum wall temperature using the numerical model does not account for the thermal resistance between the heater surface and the channel wall. Hence, the heat transfer coefficient obtained numerically is higher compared to experiment results. The results were found to satisfy the global energy balance at the inlet and outlet of the channel within 4% balance.

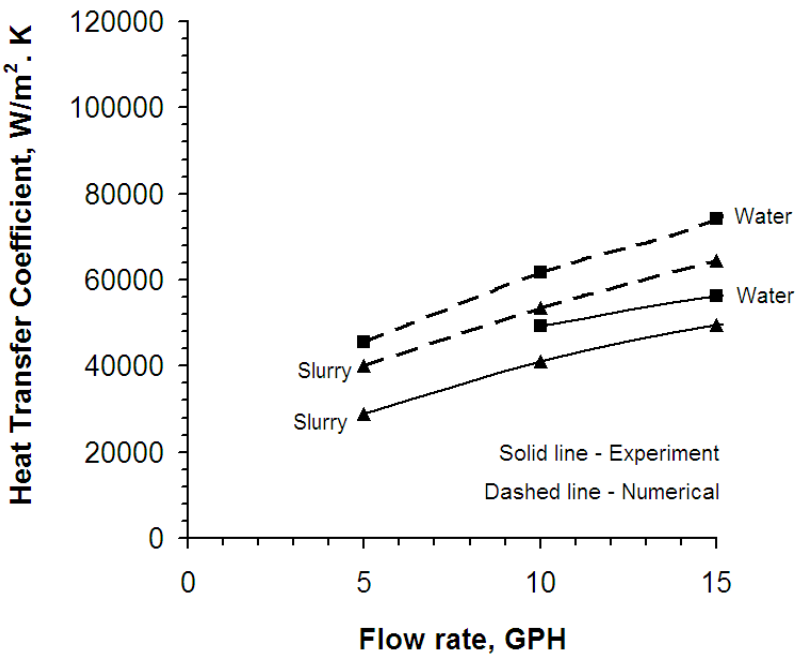

Figure 5-8. Comparison of numerical and experiment results

5.3 Results: Parametric Study – II

Based on the above results and parametric study presented in Chapter 4, it is obvious that the performance of slurry depends on the thermal conductivity of base fluid. Also, the particle size should be smaller so that the particle melts by the time it exits the channel. Since most of the fluid away from the walls did not absorb heat from the walls in case of 101 μm wide channels, simulations were also done in channels of 25 μm width. Parametric study was continued by varying the base fluid, particle concentration and channel dimensions. Table 5-6 shows the properties of suspension components used.

Table 5-6. Thermophysical properties used for parametric study – II

	Density (kg/m^3)	Specific heat (J/kg.K)	Thermal conductivity (W/m.K)	Viscosity (kg/m.s)	Latent heat (J/kg)
PAO	783	2242	0.143	$4.45x10^{-3}$	-
n-Octadecane	815	2000	0.18	-	$244x10^3$
Water	997	4180	0.604	$1x10^{-3}$	-
Copper	8700	385	400	-	-

5.3.1 Performance of water and PAO in 101 μm wide channels

PAO based slurry was used for simulations in channels used for experiment, assuming a particle diameter of 100 nm. The viscosity of the fluid was calculated using Equation 4.26, since there are no reported values of dynamic viscosity for nanoPCM based fluids. For comparison, a heat sink inlet flow rate of 10 GPH and a heat flux of 180 W/cm^2 were used for both water and PAO based fluids. The inlet temperature used is 25 ^0C, which is within the melting range. Figure 5-9 shows the bulk temperature rise predicted for both water and PAO. It can be observed that the bulk temperature rise decreases with increase in the particle mass concentration. Figure 5-10 shows the heat transfer coefficient ratio (h_r) of both water and PAO as base fluid.

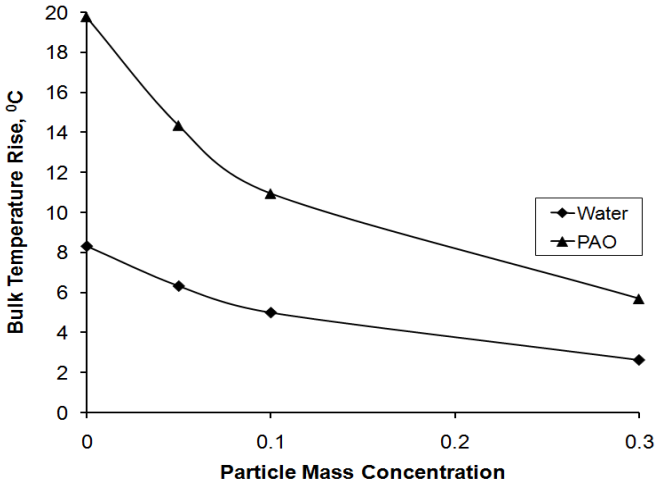

Figure 5-9. Bulk temperature rise for water and PAO

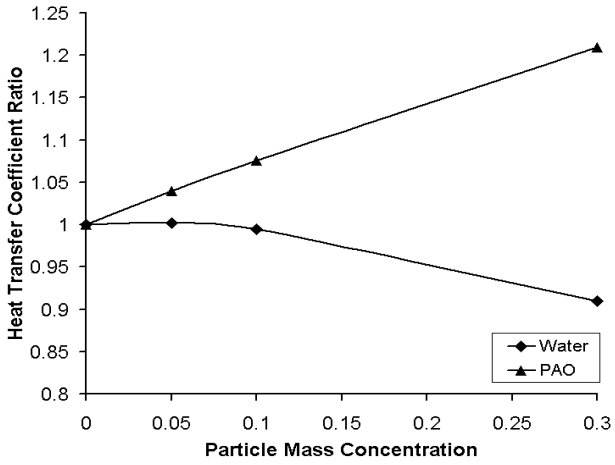

Figure 5-10. Heat transfer coefficient ratio for water and PAO

In Figure 5-10, h_{water} = 61832 W/m^2.K and h_{PAO} = 18286 W/m^2.K. The heat transfer coefficient decreases with increase in particle mass concentrations when water is used as the base fluid except with mass concentration equal to 0.05. Slight increase in heat transfer coefficient at mass concentration of 0.05 indicates that the degradation in thermal conductivity is not

significant and hence the increase in the specific heat compared to base fluid helps the slurry performance. When PAO is used as base fluid, the heat transfer coefficient increased with increase in concentration. This shows that for developing PCM slurry flows, thermal conductivity plays a very important role in determining the slurry performance.

5.3.2 Performance in 25 μm wide channels

Since most of the fluid did not absorb heat in case of 101 μm wide channels as the thermal boundary layer was not developed, smaller hydraulic diameter was used in order to aid the thermal boundary to develop faster. Hence numerical investigation was continued by using the simulation domain as configuration II (channel width 25 μm). The total number of channels inside the heat sink is 2000. An inlet flow rate of 10 GPH and heat flux of 180 W/cm^2 was used.

Figures 5-11 and 5-12 show the temperature profile of water based slurry in both the channels considered. It can be observed that in case of 101 μm wide channels, large portion of fluid did not absorb heat and in case of 25 μm wide channels, the temperature profile is more developed.

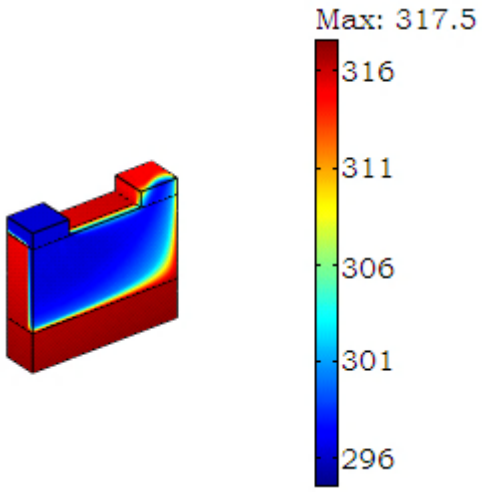

Figure 5-11. Temperature profile of water based slurry in 101 µm wide channels

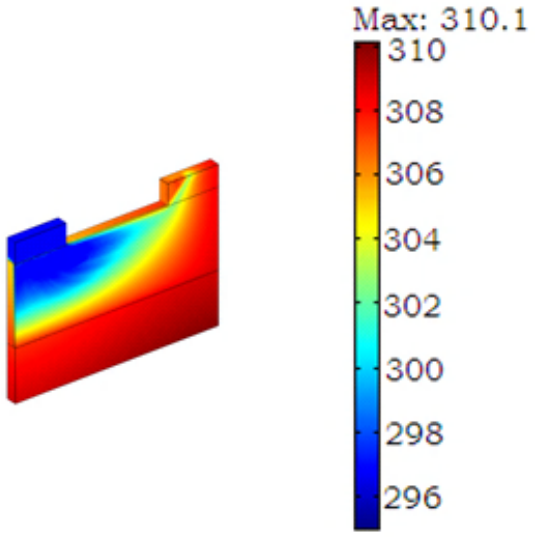

Figure 5-12. Temperature profile of water based slurry in 25 µm wide channels

Figures 5-13 and 5-14 show the bulk temperature rise and heat transfer coefficient ratio predicted with water as base fluid at different fluid inlet temperatures. The heat transfer

coefficient of slurry is 1.5 times of water at high mass concentration enabling a maximum wall temperature decrease of 4 K.

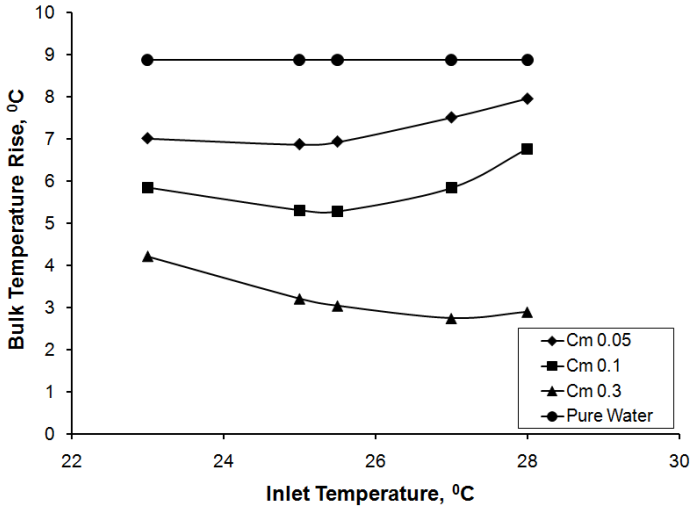

Figure 5-13. Bulk temperature rise in case of 25 µm wide channels (base fluid – water)

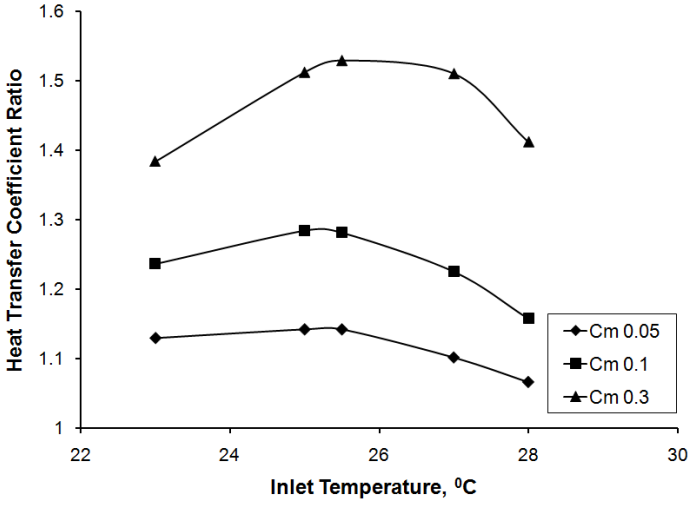

Figure 5-14. Heat transfer coefficient ratio for water (h_{water} = 150695 W/m^2.K)

Figures 5-15 and 5-16 show the bulk temperature rise obtained with PAO as base fluid and the heat transfer coefficient of PAO slurry is twice of pure PAO at high concentration. The maximum wall temperature for 30% PAO slurry is 15 K lower than the maximum wall temperature of pure PAO.

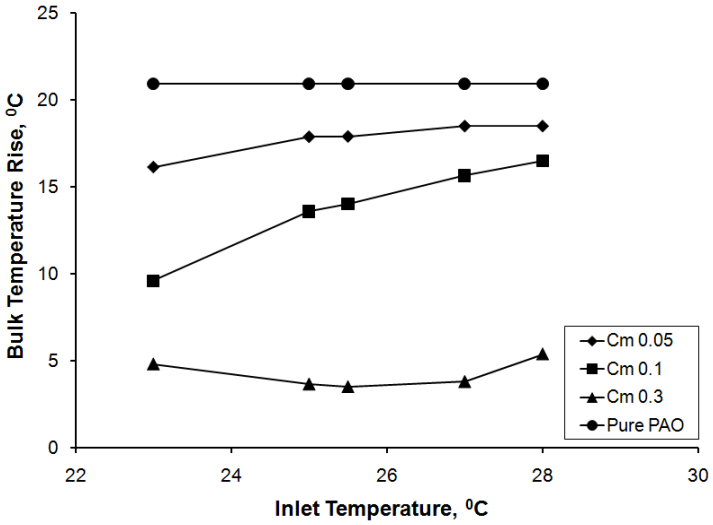

Figure 5-15. Bulk temperature rise (base fluid - PAO)

Decreasing the channel width to 25 µm allow more number of fins within the heat sink. Compared to wider channels, more amount of fluid absorbs heat within each channel and the flow is closer to thermally fully developed as the thermal entrance length is short in case of narrow channels. Hence, using smaller width channels enabling more heat transfer to the fluid helps to obtain better heat transfer coefficient for slurries compared to pure base fluid. Amount of PCM that participates in heat absorption by the time the fluid exits the channel depends on the inlet temperature. For water, if the inlet temperature is around 25.5 ^{0}C, the heat transfer coefficient is the highest, where as for PAO, it is 23 ^{0}C.

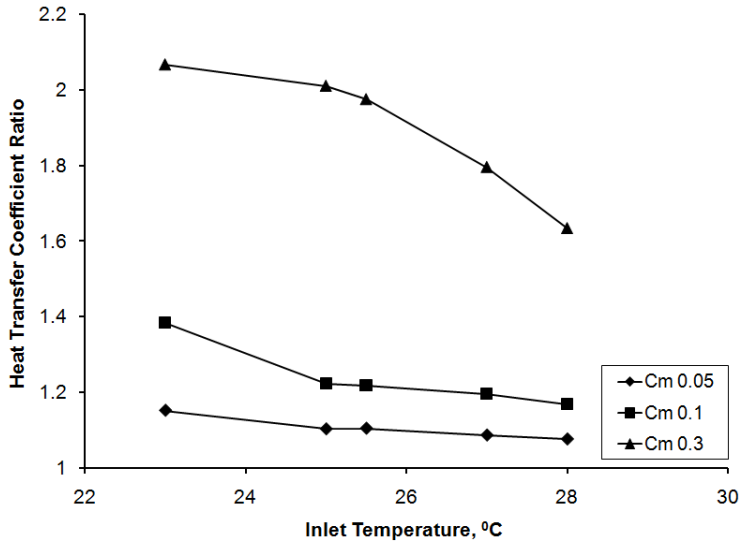

Figure 5-16. Heat transfer coefficient ratio (Base Fluid PAO, h_{PAO} = 61930 W/m^2.K)

5.3.2.1 Effect of mass concentration on pressure drop

In order to investigate the effect of high concentration on pressure drop, simulations were run using pure water and pure PAO to calculate Performance Factor (**PF**) defined as in Equation 5.2, when the heat transfer coefficient of slurry and pure base fluid is same.

$$\mathbf{PF} = \Delta P_{\text{base fluid}} / \Delta P_{\text{slurry}} \tag{5.2}$$

This parameter signifies increase or decrease in the pressure drop when a pure fluid is used in order to achieve the heat transfer coefficient as slurry. For example, the heat transfer coefficient of water based slurry at 5% concentration is 171672 W/m^2.K when the heat sink inlet flow rate is 10 GPH and heat flux is 180 W/cm^2. In order to achieve the same heat transfer

coefficient with water, a higher heat sink inlet flow rate was used and the resultant pressure drop inside the channel was 1.14 times of the pressure drop when 5% slurry was used. Figure 5-16 shows the PF with both water and PAO, when the channel width is 25 μm and heat flux is 180 W/cm^2. The heat sink inlet flow rate used for pure water and PAO is higher than 10 GPH, where as for slurry it is 10 GPH for all the concentrations.

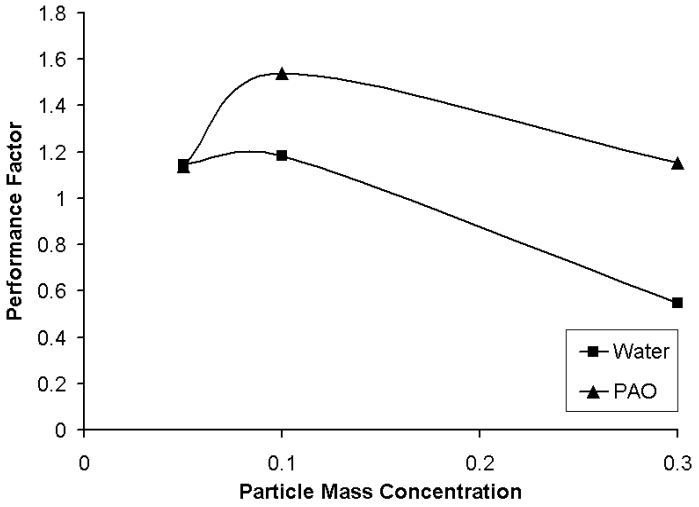

Figure 5-17. Performance factor vs c_m

For high mass concentrations, the pressure drop in case of slurry is higher compared to pure water for same heat transfer coefficient. It can be concluded that particle mass concentration of 0.1 has the highest PF for both water and PAO based slurries. It is assumed that the microchannel pressure drop dominates the total pressure drop. These results are assumed true for the parameters considered and might change with flow rate, channel dimensions, heat flux, fluid inlet temperature etc.

CHAPTER 6 : SUMMARY AND CONCLUSIONS

6.1 Summary of Results

The performance of encapsulated phase change material (EPCM) slurry flow in microchannels was investigated using the effective heat capacity method. The importance of including the particle migration inside the microchannel while solving the temperature distribution was investigated. The particle distribution was modeled using the diffusive flux model and the results were used to solve the temperature profile. In order to investigate the effect of particle migration, the thermal results obtained with and without including the particle migration were compared. For parametric study, the three dimensional flow inside the microchannels was solved including the microchannel wall/fin effects and developing flow in manifold microchannels. A constant inlet velocity and temperature were assumed along with constant heat flux condition at the base. Parametric study was done by varying parameters such as particle concentration, inlet temperature of the fluid, melting range of PCM, base heat flux and base fluid. Experiments were performed in microchannels of 101 μm width with MEPCM particle of diameter 5 μm. The results are summarized as follows.

It was found that for very short lengths (~1 mm), the migration of particles is not significant. The migration was found to depend on the ratio of particle diameter to channel width and particle concentration. The larger the particle diameter and concentration, more rapid is the particle migration. It was also found that the particle profile varied slightly when the base fluid is different.

Thermal simulations using the results of diffusive flux model showed that, when the particle migration profile is developing, the maximum wall temperature, $T_{wall,max}$ is around 1.4 K different compared to $T_{wall,max}$ obtained assuming homogeneous particle distribution. In case of water, the maximum wall temperature assuming developing profile is lower compared to the maximum wall temperature obtained assuming homogeneous distribution, where as this behavior is opposite in case of PAO. The reason can be because of the decrease or increase in overall thermal conductivity of the fluid at wall. The maximum wall temperature in case of assuming fully developed profile showed a maximum difference of 5 K compared to that of assuming homogeneous distribution. However, for obtaining such profile, the length of channel should be very long or of the order of 10 cm in the case considered which is not likely in case of microchannels (due to the associated high pressure drops).

Thermal conductivity of slurry plays a very important role in the cooling performance of slurry in microchannels, especially in manifold microchannels, which provide flow lengths that are comparable to the developing length of the flow. Results show that the heat transfer coefficient of water based slurry is lower compared to pure water when the channel width is 100 μm. For the same configuration, when the base fluid is changed to pure PAO, that has the thermal conductivity equal to that of the PCM, heat transfer coefficient of slurry is higher compared to pure PAO and the heat transfer coefficient increased with increase mass concentrations. Thus in order to achieve better performance of slurry in developing flows, presence of PCM particles should enhance the thermal conductivity of the base fluid.

Experiments were performed in microchannels of width 101 μm with water based slurry and pure water. Flow rates of water and slurry with mass concentration of 0.1 were varied

between 5 GPH and 30 GPH. Slurry performance was poor compared to pure water for all the flow rates used. The reasons for poor performance of slurry can be due to lowering of thermal conductivity in case of slurry and the large size of particles that might not have melt within the residence time.

Slurry performance depends on the geometric configuration of the microchannel. Numerical investigation showed that in microchannels of width 25 μm, water based slurry too showed high heat transfer coefficient compared to pure water at all mass concentrations. This is possibly because the flow develops faster in narrow channels.

When same heat transfer coefficient is desired with both slurry and water, results showed that higher mass concentrations are not favorable because of large pressure drop across the microchannel. Particle mass concentration of 0.1 showed the highest value of performance factor for the parameters considered.

Performance of PCM slurries in case of thermally developing flows depends on many factors. Using a PCM that can enhance the thermal conductivity of slurry, smaller MEPCM particles that can melt instantaneously, narrow channels that can help the flow develop faster, along with right inlet temperature can help to achieve maximum benefit of slurry and hence tuning of slurry parameters is very important.

6.2 Recommendations

Use of EPCM slurries as heat transfer and heat storage media is being studied in different applications. In order to analyze the slurry performance in more detail, and extend the concept to a wider range of parameters, future work may involve the following:

- Use the exact DSC curve to represent the specific heat of PCM in the numerical simulations.
- Use PCMs that have thermal conductivity much higher compared to base fluids (example: metallic alloys) and observe the effect on thermal performance.
- Perform experiments using nanoPCM slurry in MMC heat sinks to validate the numerical studies.

LIST OF REFERENCES

[1] D. B. Tuckerman, and R. F. W. Pease, "High Performance Heat Sink for VLSI," *IEEE Electron Device Lett., EDL*, vol. 2, pp. 126–129, 1981.

[2] G.M. Harpole, J.E. Eninger, "Microchannel heat exchanger optimization," Proc. 7th IEEE Semi-Therm Symp., pp. 59–63, 1991.

[3] D. Copeland, H. Takahira, and W. Nakayama, "Manifold microchannel heat sinks: theory and experiments," Therm. Sci. Eng., vol. 3, pp. 9–15, 1995.

[4] D. Copeland, M. Behnia, and W. Nakayama, "Manifold microchannel heat sinks: isothermal analysis," *IEEE Trans. On Components, Packaging, and Manufacturing Technology– – Part A,* vol. 20, pp. 96–102, 1997.

[5] Z. Lian, K. Jae-Mo, J. Linan, M. Asheghi, K. E. Goodson, J. G. Santiago, and T. W. Kenny, "Measurements and modeling of two-phase flow in microchannels with nearly constant heat flux boundary conditions," *Journal of Microelectromechanical Systems,* vol. 11, pp. 12-19, 2002.

[6] S. Kandlikar, "High flux heat removal with microchannels - A roadmap of challenges and opportunities," Proceedings of the third international conference on microchannels and minichannels, 2005.

[7] P. Charunyakorn, S. Sengupta, and S. K. Roy, "Forced convection heat transfer in microencapsulated phase change material slurries: flow in circular ducts," *International Journal of Heat and Mass Transfer*, vol. 34, pp. 819-833, 1991.

[8] D. P. Colvin, and J. C. Mulligan, "Microencapsulated phase change for storage of heat," George C. Marshall Space Flight Center NASA Tech. Brief MFSA-27198, 1987.

[9] R. Hart, and F. Thornton, "Microencapsulation of phase change materials," Ohio Department of energy, Ohio, Final report Contract No. 82-80, 1987.

[10] J. W. A. Mcmohan, J. W. W. Harlowe, and D. J. Mangold, "Feasibilty study of utilizing phase change coolant for protective garment," U.S. Army Natick Research and Development Command, Naticke, Massachusetts, Final report Contract No. DAAK60-810C-0098, 1982.

[11] K. E. Kasza, and M. M. Chen, "Improvement of the performance of solar energy or waste heat utilization systems by using phase-change slurry as an enhanced heat-transfer storage fluid," *J. Sol. Energy Eng.,* vol. 107, pp. 229-236, 1985.

[12] D. P. Colvin, and J. C. Mulligan, "Spacecraft heat rejection methods: Active and passive heat transfer for electronic systems," Flight Dynamics Laboratory, Air Force Wright Aeronautical Laboratories, Phase I, Final Report 1986.

[13] K. Chen, and M. M. Chen, "An analytical and experimental investigation of the convective heat transfer of phase change suspension flows," International Symposium on Multiphase flow, 1987.

[14] D.P. Colvin, Y.B. Bryant, J. C. Mulligan, and J. D. Duncan, "Microencapsulated phase change heat transfer system," U.S. Air Force Wright R & D center, OH WRDC-TR-89-3072, 1989.

[15] S. K. Roy, and S. Sengupta, "An evaluation of phase change microcapsules for use in enhanced heat transfer fluids," *International Communications in Heat and Mass Transfer*, vol. 18, pp. 495-507, 1991.

[16] M. Goel, S. K. Roy, and S. Sengupta, "Laminar forced convection heat transfer in microcapsulated phase change material suspensions," *International Journal of Heat and Mass Transfer*, vol. 37, pp. 593-604, 1994.

[17] J. C. Mulligan, D. P. Colvin, and Y. G. Bryant, "Use of two-component fluids of microencapsulated phase-change materials for heat transfer in spacecraft thermal systems," presented at AIAA, 1994.

[18] Y. W. Zhang and A. Faghri, "Analysis of forced convection heat transfer in microcapsulated phase change material suspensions," *J Thermophysics Heat Transfer*, vol. 9, pp. 727–732, 1995.

[19] S. K. Roy and B. L. Avanic, "Laminar forced convection heat transfer with phase change material emulsions," *International Communications in Heat and Mass Transfer*, vol. 24, pp. 653-662, 1997.

[20] Y. Yamagishi, H. Takeuchi, A. T. Pyatenko, and N. Kayukawa, "Characteristics of microencapsulated PCM slurry as a heat-transfer fluid," *AIChE Journal*, vol. 45, pp. 696-707, 1999.

[21] S. K. Roy, and B. L. Avanic, "Laminar forced convection heat transfer with phase change material suspensions," *International Communications in Heat and Mass Transfer*, vol. 28, pp. 895-904, 2001.

[22] Y. Zhang, X. Hu, and X. Wang, "Theoretical analysis of convective heat transfer enhancement of microencapsulated phase change material slurries," *Heat and Mass Transfer*, vol. 40, pp. 59-66, 2003.

[23] Y. L. Hao, and Y. X. Tao, "A numerical model for phase-change suspension flow in microchannels," *Numerical Heat Transfer, Part A,* vol. 46, pp. 55– 77, 2004.

[24] K. Q. Xing, Y. X. Tao, and Y. L. Hao, "Performance Evaluation of Liquid Flow With PCM Particles in Microchannels," *Journal of Heat Transfer*, vol. 127, pp. 931-940, 2005.

[25] B. Chen, X. Wang, Y. Zhang, H. Xu, and R. Yang, "Experimental research on laminar flow performance of phase change emulsion," *Applied Thermal Engineering*, vol. 26, pp. 1238-1245, 2006.

[26] Y. Rao, F. Dammel, P. Stephan, and G. Lin, "Convective heat transfer characteristics of microencapsulated phase change material suspensions in minichannels," *Heat and Mass Transfer*, vol. 44, pp. 175-186, 2007.

[27] X. Wang, J. Niu, Y. Li, X. Wang, B. Chen, R. Zeng, Q. Song, and Y. Zhang, "Flow and heat transfer behaviors of phase change material slurries in a horizontal circular tube," *International Journal of Heat and Mass Transfer*, vol. 50, pp. 2480-2491, 2007.

[28] B. Chen, X. Wang, R. Zeng, Y. Zhang, X. Wang, J. Niu, Y. Li, and H. Di, "An experimental study of convective heat transfer with microencapsulated phase change material suspension: Laminar flow in a circular tube under constant heat flux," *Experimental Thermal and Fluid Science*, vol. 32, pp. 1638-1646, 2008.

[29] L. Royon and G. Guiffant, "Forced convection heat transfer with slurry of phase change material in circular ducts: A phenomenological approach," *Energy Conversion and Management*, vol. 49, pp. 928-932, 2008.

[30] L. Wang, G. Lin, H. Chen, and Y. Ding, "Convective heat transfer characters of nanoparticle enhanced latent functionally thermal fluid," *Science in China Series E: Technological Sciences*, vol. 52, pp. 1744-1750, 2009.

[31] E. L. Alisetti, and S. K. Roy, "Forced Convection Heat Transfer to Phase Change Material Slurries in Circular Ducts," *Journal of Thermophysics and Heat Transfer*, vol. 14, pp. 115-118, 2000.

[32] R. Sabbah, M. M. Farid, and S. Al-Hallaj, "Micro-channel heat sink with slurry of water with micro-encapsulated phase change material: 3D-numerical study," *Applied Thermal Engineering*, vol. 29, pp. 445-454, 2009.

[33] X. Hu and Y. Zhang, "Novel insight and numerical analysis of convective heat transfer enhancement with microencapsulated phase change material slurries: laminar flow in a circular tube with constant heat flux," *International Journal of Heat and Mass Transfer*, vol. 45, pp. 3163-3172, 2002.

[34] A. S. Ahuja, "Augmentation of heat transport in laminar flow of polystyrene suspensions. II. Analysis of the data," *Journal of Applied Physics*, vol. 46, pp. 3417-3425, 1975.

[35] A. S. Ahuja, "Augmentation of heat transport in laminar flow of polystyrene suspensions. I. Experiments and results," *Journal of Applied Physics*, vol. 46, pp. 3408-3416, 1975.

[36] L. G. Leal, "On the effective conductivity of dilute suspension of spherical drops in the limit of low particle Peclet number," *Chem. Eng. Commun*, vol. 1, pp. 21-31, 1973.

[37] A. Nir and A. Acrivos, "The effective thermal conductivity of sheared suspensions," *J. Fluid Mech*, vol. 78, pp. 33-48, 1976.

[38] C. W. Sohn and M. M. Chen, "Microconvective thermal conductivity of disperse two-phase mixture as observed in a laminar flow," *J. Heat Transfer*, vol. 103, pp. 45-51, 1981.

[39] Segre, G., and A. Silberberg, "Behaviour of macroscopic rigid spheres in Poiseuille flow Part 2. Experimental results and interpretation," *Journal of Fluid Mechanics Digital Archive*, vol. 14, pp. 136-157, 1962.

[40] S. A. Altobelli, R. C. Givler, and E. Fukushima, "Velocity and concentration measurements of suspensions by nuclear magnetic resonance imaging," *Journal of Rheology*, vol. 35, pp. 721-734, 1991.

[41] E. S. Boek, P. V. Coveney, H. N. W. Lekkerkerker, and P. van der Schoot, "Simulating the rheology of dense colloidal suspensions using dissipative particle dynamics," *Physical Review E*, vol. 55, pp. 3124, 1997.

[42] D. Leighton, and A. Acrivos, "The shear-induced migration of particles in concentrated suspensions," *Journal of Fluid Mechanics Digital Archive*, vol. 181, pp. 415-439, 1987.

[43] P. R. Nott, and J. F. Brady, "Pressure-driven flow of suspensions: simulation and theory," *Journal of Fluid Mechanics Digital Archive*, vol. 275, pp. 157-199, 1994.

[44] S. Chen, and G. D. Doolen, "Lattice Boltzmann method for fluid flows," *Annual Review of Fluid Mechanics*, vol. 30, pp. 329, 1998.

[45] J. R. Abbott, N. Tetlow, A. L. Graham, S. A. Altobelli, E. Fukushima, L. A. Mondy, and T. S. Stephens, "Experimental observations of particle migration in concentrated suspensions: Couette flow," *Journal of Rheology*, vol. 35, pp. 773-795, 1991.

[46] C. J. Koh, P. Hookham, and L. G. Leal, "An experimental investigation of concentrated suspension flows in a rectangular channel," *Journal of Fluid Mechanics Digital Archive*, vol. 266, pp. 1-32, 1994.

[47] R. Glowinski, T. W. Pan, T. I. Hesla, and D. D. Joseph, "A distributed Lagrange multiplier/fictitious domain method for particulate flows," *International Journal of Multiphase Flow*, vol. 25, pp. 755-794, 1999.

[48] A. W. Chow, S. W. Sinton, and J. H. Iwamiya, "Direct observation of particle microstructure in concentrated suspensions during the falling-ball experiment," *Journal of Rheology*, vol. 37, pp. 1-16, 1993.

[49] R. J. Phillips, R. C. Armstrong, R. A. Brown, A. L. Graham, and J. R. Abbott, "A constitutive equation for concentrated suspensions that accounts for shear-induced particle migration," *Physics of Fluids A: Fluid Dynamics*, vol. 4, pp. 30-40, 1992.

[50] I. M. Krieger, "Rheology of monodisperse latices," *Advances in Colloid and Interface Science*, vol. 3, pp. 111-136, 1972.

[51] C. Kim, "Mathematical model of migration of spherical particles in tube flow under the influence of inertia and particle-particle interaction," *Korean Journal of Chemical Engineering*, vol. 21, pp. 27-33, 2004.

[52] R. E. Hampton, A. A. Mammoli, A. L. Graham, N. Tetlow, and S. A. Altobelli, "Migration of particles undergoing pressure-driven flow in a circular conduit," *Journal of Rheology*, vol. 41, pp. 621-640, 1997.

[53] D. Semwogerere, J. F. Morris, and E. R. Weeks, "Development of particle migration in pressure-driven flow of a Brownian suspension," *Journal of Fluid Mechanics*, vol. 581, pp. 437-451, 2007.

[54] A. Karnis, H. L. Goldsmith, S. G. Mason, The kinetics of flowing dispersions. I. Concentrated suspensions of rigid particles, J. Colloid. Interf. Sci., 22: 531–553, 1966.

[55] R.W. Watkins, C. R. Robertson, and A. Acrivos, “Entrance region heat transfer in flowing suspensions,” *Int. J. Heat Mass Transfer,* vol. 19, pp. 693-695, 1976.

[56] L. C. Tao, "Generalized numerical solutions of freezing a saturated liquid in cylinders and spheres," *AIChE Journal*, vol. 13, pp. 165-169, 1967.

[57] J. C. Maxwell, *A Treatise on Electricity and Magnetism 1,* vol. 1, 3 ed. New York: Dover Publications, Inc., 1954.

[58] E. Yamada and K. Takahashi, "Effective Thermal Conductivity of Suspensions - 1st Report," *Hear Transfer: Japanese Research*, vol. 4, pp. 83-101, 1975.

[59] www.comsol.com

[60] H. Schlichting, K.Gersten, E. Krause, and H. Jr. Oertel, *Boundary Layer Theory,* 8th edition, Springer, New York, NY, 2000.

[61] I. R. Rutgers, "Relative viscosity of suspensions of rigid spheres in Newtonian liquids," *Rheologica Acta*, vol. 2, pp. 202-210, 1962.

[62] V. Vand, "Theory of viscosity of concentrated suspensions," *Nature*, vol. 155, pp. 364-365, 1945.

[63] V. Vand, "Viscosity of solutions and suspensions," *J. Phys. Coll. Chem*, vol. 52, pp. 300-321, 1948.

[64] C. B. Gu, G. S. Su, L. C. Chow, and M. R. Pais, "Comparison of spray and jet impingement cooling," National Heat Transfer Conference, 1993.

[65] Z. Duan and Y. Muzychka, "Impingement air cooled plate fin heat sinks, part-I, pressure drop model," Intersociety Conference on Thermal Phenomena, 2004.

[66] www.matlab.com